



Variations in O₃, CO, and CH₄ over the Bay of Bengal during the summer monsoon season: Ship-borne measurements and model simulations

5 Imran A. Girach^{1,2}, Narendra Ojha², Prabha R. Nair¹, Andrea Pozzer², Yogesh K. Tiwari³, K. Ravi Kumar^{4,5}, and Jos Lelieveld²

¹Space Physics Laboratory, Vikram Sarabhai Space Centre, Thiruvananthapuram 695022, India

²Department of Atmospheric Chemistry, Max Planck Institute for Chemistry, Mainz 55128, Germany

³Indian Institute of Tropical Meteorology, Pune 411 008, India

10 ⁴National Institute of Polar Research, Tachikawa, Japan

⁵Department of Environmental Geochemical Cycle Research, JAMSTEC, Yokohama, Japan

Correspondence to: Imran A. Girach (imran.girach@gmail.com) and Narendra Ojha (narendra.ojha@mpic.de)

15 **Abstract**

We present ship-borne measurements of surface ozone, carbon monoxide and methane over the Bay of Bengal (BoB), the first time such measurements have been taken during the summer monsoon season, as a part of the Continental Tropical Convergence Zone (CTCZ) experiment during 2009. O₃, CO, and CH₄ mixing ratios exhibited significant spatial and temporal variability in the ranges of 8–54 nmol mol⁻¹, 50–200 nmol mol⁻¹, and 1.57–2.15
20 μmol mol⁻¹, with means of 29.7±6.8 nmol mol⁻¹, 96±25 nmol mol⁻¹, and 1.83±0.14 μmol mol⁻¹, respectively. The average mixing ratios of trace gases over northern BoB (O₃: 30±7 nmol mol⁻¹, CO: 95±25 nmol mol⁻¹, CH₄: 1.86±0.12 μmol mol⁻¹), in airmasses from northern or central India, did not differ much from those over central BoB (O₃: 27±5 nmol mol⁻¹, CO: 101±27 nmol mol⁻¹, CH₄: 1.72±0.14 μmol mol⁻¹), in airmasses from southern India. Spatial variability is observed to be most significant for CH₄. The ship-based observations, in conjunction with
25 backward air trajectories and ground-based measurements over the Indian region, are analyzed to estimate a net ozone production of 1.5–4 nmol mol⁻¹ day⁻¹ in the outflow. Ozone mixing ratios over the BoB showed large reductions (by ~20 nmol mol⁻¹) during four rainfall events. Temporal changes in the meteorological parameters, in conjunction with ozone vertical profiles, indicate that these low ozone events are associated with downdrafts of free-tropospheric ozone-poor airmasses. While the observed variations in O₃ and CO are successfully reproduced using
30 the Weather Research and Forecasting model with Chemistry (WRF-Chem), this model overestimates mean concentrations by about 20%, generally overestimating O₃ mixing ratios during the rainfall events. Analysis of the chemical tendencies from model simulations for a low-O₃ event on August 10, 2009, captured successfully by the model, shows the key role of horizontal advection in rapidly transporting ozone-rich airmasses across the BoB. Our



study fills a gap in the availability of trace gas measurements over the BoB, and when combined with data from
35 previous campaigns, reveals large seasonal amplitude (~ 39 and ~ 207 nmol mol⁻¹ for O₃ and CO, respectively) over
the northern BoB.

1. Introduction

Tropospheric ozone (O₃) is the third most important greenhouse gas, contributing to global warming and climate
40 change with its radiative forcing of 0.40 ± 0.20 Wm⁻² (IPCC 2013). O₃ is also a pivotal trace gas in tropospheric
chemistry, as it is a major source of hydroxyl radical (OH), which removes most of the organic compounds and
pollutants from the atmosphere and controls the oxidation capacity of the troposphere (e.g. Brasseur et al., 1999;
Finlayson-Pitts and Pitts, 2000; Seinfeld and Pandis, 2006). Further, enhanced concentrations of surface O₃ have
45 detrimental effects on human health and vegetation (Heagle, 1989; Seinfeld and Pandis, 2006). Approximately 80%
of tropospheric O₃ is produced by in situ photochemical reactions in the presence of nitrogen oxides (NO_x = NO +
NO₂) involving the precursor gases of methane, non-methane hydrocarbons (NMHCs), and CO (Fishman et al.,
1979; Crutzen et al., 1999; Seinfeld and Pandis, 2006). The remaining 20% of tropospheric ozone is attributed to
intrusions of stratospheric air during frontal activities or to tropopause folding events (Lelieveld and Dentener, 2000;
50 Sprenger et al., 2007). Depending upon meteorological conditions and the availability of the aforementioned
precursors, a net production or destruction of O₃ prevails. The average lifetime of ozone is about one week in the
lower troposphere, which leads to large variability in its spatial and temporal distributions, as compared to the long-
lived greenhouse gases. The budget of tropospheric ozone and its implications for human health, crop yields, and
climate are, however, not yet well quantified, especially over regions in Asia. This is mainly due to insufficient in
situ measurements (e.g. Cooper et al., 2014; Monks et al., 2015).

55 Carbon monoxide (CO) is an indirect greenhouse gas which also has adverse effects on humans and animals (WHO
1999). Although it does not have a direct greenhouse effect like methane or carbon dioxide, its role in atmospheric
chemistry is estimated to cause an indirect radiative forcing of 0.23 (0.18 – 0.29) Wm⁻² (IPCC 2013). The major
sources of CO are fossil fuel combustion, biomass burning, and oxidation of hydrocarbons such as CH₄ and isoprene
(e.g. Jacob, 1999; Bergamaschi et al., 2000; Seinfeld and Pandis, 2006).

60 Methane (CH₄) is one of the major greenhouse gases, with a direct radiative forcing of 0.48 ± 0.05 Wm⁻² (IPCC
2013). This gas plays a major role in the climate and in atmospheric chemistry. CH₄ is emitted from variety of
natural and anthropogenic sources (Jacob, 1999) and is removed primarily through its reaction with OH radicals
(Fung et al., 1991, Seinfeld and Pandis, 2006).

The marine regions adjoining South Asia, despite being far from direct anthropogenic activities, have been observed
65 to have elevated levels of surface O₃ due to the outflow of continental pollution (Lawrence and Lelieveld, 2010) and
minimal chemical loss by titration (e.g. Lal and Lawrence, 2001; Ojha et al., 2012). Suggested sources for this
elevated ozone and other trace gases observed over the marine regions surrounding India are anthropogenic, biomass
burning, and biogenic emissions over continental India (Naja et al., 2004; Lawrence and Lelieveld, 2010; Nair et al.,



2011; David et al., 2011). The airmasses exposed to continental emissions undergo chemical transformation, including ozone production, during their transport to the cleaner marine regions. In situ measurements over the marine regions adjacent to the South Asia are therefore required to understand the chemistry in the airmasses transported to the marine regions, the effects of direct outflow, and en route chemical transformation. (Lawrence and Lelieveld, 2010, and references therein).

The experiments that have been conducted to date over the marine environment adjacent to the Indian region have revealed considerable spatial heterogeneity in the distribution of trace gases and aerosols, influences from source regions such as the Indo-Gangetic Plains (IGP), and radiative impacts (Nair et al., 2011; David et al., 2011; Mallik et al., 2013; Moorthy et al., 2009; Nair et al., 2010). Observations made during the Indian Ocean Experiment (INDOEX; Lal and Lawrence, 2001) and model simulations (Ojha et al., 2012) both found the ozone mixing ratios over these remote marine regions to be even higher than those over the upwind continental regions, due to complex ozone chemistry. Lawrence and Lelieveld (2010) provided a detailed review of the outflow of trace gases and aerosols from South Asia to the surrounding marine regions. Both the export of continental airmasses and the transport of marine air to the continental regions have strong seasonal dependence associated with the changes in synoptic scale dynamics and monsoonal circulations (e.g. Kumar et al., 2015).

The marine environment of the Bay of Bengal (BoB), the largest bay in the world, is surrounded by landmasses on three sides, making it highly conducive for the accumulation of trace species. Further, seasonal changes in synoptic winds make this a unique region to study variations in trace species due to transport and en route photochemistry. Considering the aforementioned special characteristics of the BoB, as well as the considerable heterogeneity of trace gas and aerosol distribution, in situ measurements covering large areas are essential for investigating the distribution of pollutants and the controlling processes. Extensive in situ measurements of various trace gases over the BoB have been conducted in the following field campaigns: INDOEX during the winter months of 1998 and 1999 (Lelieveld et al., 2001; Muhle et al., 2002); the Integrated Campaign for Aerosols, gases, and Radiation Budget (ICARB) during the March–May (pre-monsoon season) of 2006 (Nair et al., 2011; Srivastava et al., 2011; Srivastava et al., 2012); the winter-ICARB (W-ICARB) during December–January 2009 (Girach and Nair, 2010; 2014; David et al., 2011); the Bay of Bengal Experiment (BOBEX)-I during February–March 2001 (Lal et al., 2006); the Bay of Bengal Process Studies (BOBPS) during September–October 2002 (Sahu et al., 2006); BOBEX-II during February 2003 (Lal et al., 2007); and an unnamed campaign conducted during October–November 2010 (Mallik et al., 2013).

Although earlier studies have covered the spatio-temporal distribution of trace gases during most seasons over the BoB, there is still a lack of observations over the BoB during the summer monsoon season (June–August). Asian summer monsoon circulation provides a pathway for pollution transport into the stratosphere (Randel et al., 2010), and observations taken during monsoon season capture a time of high water-vapour loading over the BoB, which influences the oxidation capacity of the atmosphere. Deep convection during the summer monsoon can uplift boundary layer pollution to higher altitudes, which is then distributed over a larger region, thereby influencing air quality and climate over much larger regions (Lawrence and Lelieveld, 2010), extending as far as, for example, over the Mediterranean (e.g. Lelieveld et al., 2002; Scheeren et al., 2003). Such in situ measurements are also essential



given the fact that remote sensing of boundary layer ozone using, for example, the Tropospheric Emission Spectrometer (www.tes.jpl.nasa.gov) on board the Aura satellite, has relatively higher uncertainty (Verstraeten et al., 2013). The uncertainties in satellite retrievals of trace species are particularly high during the summer monsoon season, as the view of satellite instruments is frequently obscured by thick clouds.

110 In the present paper, we present ship-based measurements of surface O₃, CO, and CH₄ over the BoB for the year 2009, the first time such measurements have been taken during the summer monsoon season in this region. These observations were carried out as a part of the Continental Tropical Convergence Zone (CTCZ) experiment (<http://odis.incois.gov.in/index.php/project-datasets/ctcz-programme>) under the Indian Climate Research Programme (ICRP) of the Government of India. In this study, we analyse the spatial and temporal variations in
115 ozone over the BoB and the effects of transport. These observations are compared with simulations from a regional model, Weather Research and Forecasting coupled with Chemistry (WRF-Chem). We investigate sharp reductions that we have observed in O₃ during rainfall events in greater detail.

The manuscript begins with a description of the ship cruise in Section 2, followed by experimental setup and observations in Section 3, description of model simulations in Section 4, and results of the study in Section 5. A
120 summary and main conclusions are presented in Section 6.

2. The cruise track and background conditions

Figure 1 shows the cruise track of the Oceanic Research Vessel (RV) *Sagar Kanya* during the CTCZ experiment (cruise number SK 261). The arrows show the direction of the ship, which sailed from Chennai (80.3° E, 13.1° N)
125 on July 16, 2009. The cruise offered greater coverage in the northern BoB than the southern or central BoB areas. To take time series measurements, the ship was kept stationary at 89° E, 19° N for fifteen days (July 22 to August 06, 2009). After several tracks, covering latitude sector 11.0 to 21.1° N and longitude sector 80.3 to 90.1° E, the cruise ended on August 17, 2009 at Chennai, for a total of 32 days of voyage. The average prevailing wind patterns at 925 hPa during the cruise period are obtained from NCEP/NCAR reanalysis (<http://www.esrl.noaa.gov/psd>; Fig. 1). The
130 prevailing westerly or south-westerly winds are conducive for the transport of ozone and its precursors from the Indian landmass to the BoB during the summer monsoon season. The spatial distribution of emissions of NO_x, an ozone precursor gas, is also shown as colour map in Fig. 1. NO_x emissions are obtained from the Intercontinental Chemical Transport Experiment – Phase B (INTEX-B) inventory (Zhang et al., 2009), which is representative of the year 2006. Relatively high NO_x emissions are located over parts of eastern and southern India.

135

3. Experimental details and data

Surface O₃ measurements were carried out using an online ultraviolet (UV) photometric ozone analyzer (Model O3 42), manufactured by Environnement S.A, France. The analyser utilises the absorption of UV radiation by ozone molecules at 253.7 nm and derives ozone mixing ratios using the Beer–Lambert law. This UV absorption-based
140 analyser has an uncertainty of about 5% (Tanimoto, 2007), corresponding to ~1.5 nmol mol⁻¹ for the observed range of ozone. Zero noise of the instrument is 0.5 nmol mol⁻¹. The instrument has a lower detection limit of 1 nmol mol⁻¹



and a linearity of $\pm 1\%$. An individual measurement is performed at a minimum response time of 10 seconds. The analyzer was operated on auto-response mode, whereby responses could 10–90 seconds depending upon changes in ozone mixing ratios. However, data were recorded continuously at 5-minute intervals.

145 CO measurements were made using an online CO analyzer (Model CO12 Module) manufactured by Environnement S.A, France. This instrument was based on the principle of Non-Dispersive Infrared (NDIR) absorption by CO molecules at the wavelength of $4.67 \mu\text{m}$. The instrument has a lower detection limit of 50 nmol mol^{-1} , a linearity of 1%, and a response time of 40 seconds. The overall uncertainty in hourly CO measurements is estimated to be $\sim 10\%$ at a CO value of $150 \text{ nmol mol}^{-1}$ (Sawa et al., 2007; Tanimoto et al., 2007).

150 Air was drawn from a height of approximately 15 meter above the sea surface through a Teflon tube. Before and after the cruise, both analyzers were calibrated, with calibration factors not found to be significantly changed. Meteorological parameters such as pressure, temperature, and relative humidity were measured continuously onboard the ship. Trace gas measurements affected by the ship exhaust were identified and discarded using onboard wind direction measurements.

155 In addition, a total of 29 air samples were collected in 1-liter glass flasks during the cruise and were analyzed for methane using a Gas Chromatograph (GC) coupled with a Flame Ionization Detector (FID), as described in Tiwari and Ravi Kumar (2011). These methane measurements are traceable to the WMO standard scale. Methane standards were obtained from the WMO Central Calibration Laboratory (CCL) at the National Oceanic and Atmospheric Administration (NOAA)/Earth System Research Laboratory (ESRL)/Global Monitoring Division (GMD), located in

160 Boulder, Colorado, USA. The precision for methane measurements was approximately $\pm 0.1 \mu\text{mol mol}^{-1}$. A detailed description of the analytical procedure for methane measurement is given in Ravikumar et al. (2014). Using the same ozone analyzer as the one used for surface O_3 measurements over BoB, continuous measurements of surface O_3 were taken at Thumba, Thiruvananthapuram (David and Nair, 2011; Girach et al., 2012) in July 2011. Along with various meteorological parameters, rainfall measurements were also taken at Thumba at 5-minute

165 accumulation intervals using an automatic weather station manufactured by Dynalab Weathertech Pvt. Ltd, India. The site, Thumba, is situated just $\sim 500 \text{ m}$ away from the west coast, with sandy terrain, and is a less populated area in the city of Thiruvananthapuram (8.5° N , 76.9° E) at southern tip of India. For more details about the Thumba site and measurements please see, for example, Nair et al. (2002) and David and Nair (2011). A vertical profile of O_3 was measured on July 28, 2011 at Thumba using an electrochemical concentration cell

170 ozonesonde (EN-SCI 2ZV7 ECC; Komhyr, 1969, 1995). The accuracy of such ozonesondes is reported to be about $\pm 5\text{--}10\%$ up to $\sim 30 \text{ km}$ (Smit et al., 2007). More details of this measurement technique can be found in Ojha et al. (2014). The accumulated rainfall for every 3-hour interval from the Tropical Rainfall Measuring Mission (TRMM; with a horizontal grid size of $0.25^\circ \times 0.25^\circ$) is also utilized in this study to complement the onboard rainfall measurements.

175 The 3B42 algorithm is used to calculate precipitation and root-mean-square precipitation-error estimates; these two estimates were then used to compute hourly and daily rainfall estimates (Huffman et al., 1995).

4. Model Simulations



The Weather Research and Forecasting model with Chemistry (WRF-Chem; Grell et al., 2005) version-3.5.1 was used to simulate meteorological and chemical fields during the campaign period. The model domain (Fig. 2) is defined on the Mercator projection, centred at 86° E, 16° N, at a spatial resolution of 15 km x 15 km. The model has 51 vertical levels from surface to 10 hPa. The simulations were conducted for the period of June 29 to August 31, 2009, covering the complete measurement period. The meteorological inputs have been adopted from ERA-interim reanalyses by the ECMWF. Horizontal winds, temperature, and water vapour are nudged above the planetary boundary layer using a nudging coefficient of 0.0003 s⁻¹ (Kumar et al., 2015), employing the Four Dimensional Data Assimilation (FDDA) technique. Anthropogenic emissions of CO, NO_x, SO₂, and NMVOCs are provided by a regional emission inventory that was developed to support the Intercontinental Chemical Transport Experiment – Phase B (INTEX-B; Zhang et al., 2009; Kumar et al., 2012b). This inventory is representative of the year 2006. Aerosol emissions are provided by the Hemispheric Transport of Air Pollution (HTAP v2) inventory (Janssens-Maenhout et al., 2015). Biomass burning emissions from NCAR Fire Inventory (FINN; Wiedinmyer et al., 2011), and biogenic emissions calculated online using MEGAN (Guenther et al., 2006) were used in the simulations. Gas-phase chemistry in the model is represented by the second-generation Regional Acid Deposition Model (RADM2; Stockwell et al., 1990), and the aerosol module is based on MADE SORGAM (Binkowski and Shankar, 1995; Ackermann et al., 1998; Schell et al., 2001). Initial and boundary conditions for chemical fields are provided by the MOZART-4/GEOS5 data. The options used to parameterize different atmospheric processes are given in Table 1. For more information about meteorological nudging, chemical mechanisms, emissions, boundary conditions, and evaluation of WRF-Chem against in situ measurements and satellite data over the Indian region, please see, for example, Kumar et al. (2012a; 2012b; 2015), Ansari et al. (2016), and Ojha et al. (2016). Model-simulated mean spatial distributions of O₃ and CO over the model domain during the study period are shown in Figure 2.

5. Results and Discussion

5.1 Variations in O₃, CO, and CH₄ over the BoB

Figure 3 shows the observed variations in O₃, CO, and CH₄ along the ship track during the July 16 to August 17, 2009 period of the summer monsoon season. In Figure 3, the solid black lines define two regions, central BoB (80–91° E, 11–16° N) and northern BoB (81–91° E, 16–21.5° N). All of the measured trace gases show significant spatio-temporal heterogeneity over the BoB region during the summer monsoon season. O₃ levels are found to vary from as low as 8 nmol mol⁻¹ to as high as 54 nmol mol⁻¹, with average mixing ratio derived from the complete data of 29.7±6.8 nmol mol⁻¹. CO mixing ratios are observed to be in the range of 50 nmol mol⁻¹ falling below the detection limit of the instrument to 198 nmol mol⁻¹, with an average value of 96±25 nmol mol⁻¹ from all observations. As CO mixing ratios below the detection limit of the instrument are discarded from the analysis, the reported minimum and average values of CO mixing ratios are therefore slightly higher than their actual values. CH₄ mixing ratios are observed to range from 1.57–2.15 μmol mol⁻¹, with average of 1.83±0.14 nmol mol⁻¹. We further separated the observations into two defined geographical regions: northern BoB and central BoB (Figure 3). The average mixing ratios for O₃, CO, and CH₄ are observed to be ~ 30±7 nmol mol⁻¹, 95±25, nmol mol⁻¹, and 1.86±0.12 μmol mol⁻¹,



respectively, over northern BoB. These ratios are comparable or only slightly higher than those over central BoB: O_3 : $27 \pm 5 \text{ nmol mol}^{-1}$, CO : $101 \pm 27 \text{ nmol mol}^{-1}$, and CH_4 : $1.72 \pm 0.14 \mu\text{mol mol}^{-1}$. Average CH_4 mixing ratios, however, showed a significant difference of $0.14 \mu\text{mol mol}^{-1}$ between northern and central BoB during the summer monsoon season.

220 In addition to sailing across the BoB, the ship was also kept stationary for fifteen days, from July 22 to August 06, 2009 at 89° E , 19° N . During this time period, surface O_3 , CO , and CH_4 mixing ratios are observed to fall into the range of $9\text{--}46 \text{ nmol mol}^{-1}$, $58\text{--}144 \text{ nmol mol}^{-1}$, and $1.71\text{--}1.89 \mu\text{mol mol}^{-1}$, respectively, with temporally averaged mixing ratios of $28 \pm 7 \text{ nmol mol}^{-1}$, $91 \pm 19 \text{ nmol mol}^{-1}$, and $1.81 \pm 0.06 \mu\text{mol mol}^{-1}$, respectively.

225 The HYbrid Single Particle Lagrangian Integrated Trajectory (HYSPLIT) model was used to simulate five-day backward airmass trajectories arriving at 500 m (a height that falls within the marine atmospheric boundary layer) above the measurement locations (Draxler and Rolph, 2003; Rolph, 2003; <http://www.arl.noaa.gov/ready.html>), as shown in the Fig. 4. Trajectories are colour-coded to show the altitude variations of the air-parcel along its path. The influences of two different airmasses are observed over the BoB during the CTCZ experiment. Over central BoB, the backward air trajectories are seen to cross southern India (i.e. $<13^\circ \text{ N}$), where a belt of elevated anthropogenic emissions ($5\text{--}20 \text{ mol km}^{-2} \text{ hr}^{-1}$ of NO_x ; see Fig. 1) is located. In contrast, most of the air trajectories over northern

230 BoB come through the central Indian region, where anthropogenic emissions are significantly lower. For example, with the exception of a few hotspots, NO_x emissions above 13° N are in the range of $1\text{--}10 \text{ mol km}^{-2} \text{ hr}^{-1}$ (Fig. 1). The observed spatio-temporal variations in the trace gases are investigated by calculating the percentage residence time of airmasses over land, using HYSPLIT simulated 5-day backward air trajectories. Figure 5a–c shows the temporal variations in O_3 , CO , and CH_4 during the CTCZ experiment along the cruise track. The percentage residence time of airmasses over continental India is also shown (blue line), as estimated by the ratio of residence time over land to the total trajectory time of 5 days. Red vertical bars depict the sharp reductions in O_3 as well as CO mixing ratios associated with rainfall events (see Section 5.4). Similar variations in O_3 mixing ratios and residence time over continental India indicate the influences of transport from the Indian subcontinent on the observed spatio-temporal variations over the BoB during the summer monsoon season. The occasions on which such a one-to-one

240 correspondence are not observed can be attributed to varying source strengths, vertical mixing or dilution, and en route photochemistry. As seen in Fig. 5b, CO is also associated with residence time, although not as strongly as in the case of O_3 . CH_4 does not show a considerable correlation with residence time over the Indian subcontinent (Fig. 5a).

245 Generally, during the summer monsoon season, relatively cleaner marine airmasses from the Arabian Sea are transported to the Indian region. These airmasses are then exposed to regional emissions and subjected to photochemistry depending upon the availability of solar insolation under the cloudy conditions of monsoon. The airmasses in which precursors have accumulated, and to some extent photo-chemically processed, outflows into the BoB. As a result, the airmasses out-flowing at the eastern coast of India could have higher ozone mixing ratios than the background air coming from the Arabian Sea into the western coast of India. The difference between these two

250 values is a representative of the ozone build-up that can be attributed to regional pollution; this difference would also reflect the extent of photochemical processing that would have taken place.



As the observational site Thumba, Thiruvananthapuram, is situated just at the Arabian Sea coast, the monsoon-time observations here could be approximated to represent the background ozone mixing ratios entering from the Arabian Sea. In August 2009, using only daytime monthly average O_3 , the ozone at Thumba during the monsoon season was observed to be 23 ± 7 nmol mol^{-1} . Since the objective of investigation is the additional O_3 over the BoB produced by en route photochemistry, daytime O_3 values at Thiruvananthapuram are therefore compared with all the observations over the BoB. The average mixing ratio observed over the BoB during monsoon season for July 16–August 17, 2009 was 30 ± 7 nmol mol^{-1} , which was ~ 7 nmol mol^{-1} higher than the Arabian Sea airmass. This additional amount of ~ 7 nmol mol^{-1} could be attributed to the effects of regional and en route photochemical ozone production. Net ozone production rate in the outflow is estimated to be in the range of 1.5 – 4 $\text{nmol mol}^{-1} \text{ day}^{-1}$ (Fig. 6). Note that the ozone mixing ratio is reported to be $\sim 30 \pm 2$ nmol mol^{-1} during July 2009 over Ananthapur, a rural site in central India, indicating the enhancement due to regional ozone production (Fig. 6). As shown in Table 2, while average O_3 mixing ratios over the west coast of India and the Arabian Sea are in the range of 9 – 25 nmol mol^{-1} during the monsoon season, the average O_3 mixing ratio is ~ 30 nmol mol^{-1} over the central Indian station and the BoB. As shown in Fig. 6, during the cruise observations, O_3 mixing ratios were 27 ± 3 and 28 ± 5 nmol mol^{-1} for July 21, 2009 and August 15, 2009, for which back-trajectories crossed Thiruvananthapuram on July 20, 2009 and August 13, 2009, with daytime O_3 values of 23 ± 6 and 25 ± 6 nmol mol^{-1} , respectively. The difference of 3 – 4 nmol mol^{-1} between ozone mixing ratios over the BoB and Thiruvananthapuram represents the en route photochemical production of ozone in the airmasses toward the observation points over the BoB. It is further found that the airmasses were typically below 700 meters, and generally within the marine boundary layer (e.g. mean boundary layer height ~ 897 m during winter over the BoB; Subrahmanyam et al., 2012). The enhancements in O_3 are attributed here to in situ photochemical build-up while moving towards the BoB, which has been noted in previous experiments and model simulations (e.g. Lal and Lawrence, 2001; Ojha et al., 2012). CO showed a sharp enhancement (denoted with red arrows in Fig. 5b) on August 7 and 11, 2009, coinciding with a longer residence time over the Indian region. Figure 7 shows backward airmass trajectories above the measurement locations, along with the distribution of anthropogenic CO emissions from the INTEX-B inventory, representative of the year 2006. The airmasses over the BoB are found to be influenced by emission hotspots (corresponding emission of 250 – 350 $\text{mol km}^{-2} \text{ hr}^{-1}$). The airmasses took about half a day to be transported from the emission hotspot to the observation location over the BoB. CO mixing ratios measured at Bhubaneswar (20.30° N; 85.83° E), a station within the hotspot region, is $\sim 251 \pm 58$ nmol mol^{-1} during the monsoon season (June–August 2011–2012; Mahapatra et al., 2014), with the elevated CO emissions in the Bhubaneswar region being attributed to industrial activities. The higher CO mixing ratios ~ 200 nmol mol^{-1} is inline with the monsoonal values observed at Bhubaneswar. The CO mixing ratios around 150 nmol mol^{-1} were sampled on August 11, 2009 near the coastal source regions. Additionally, CO mixing ratios over central BoB (101 nmol mol^{-1}) were only slightly higher than those over northern BoB (95 nmol mol^{-1}). We suggest that this is partially due to higher emissions over southern India, against the shorter residence of airmasses over land and the relatively longer lifetime of CO.

5.2 WRF-Chem simulations



290 WRF-Chem simulations, as described in Section 4, are used to evaluate the performance of the model in reproducing
our measurements, and to investigate the underlying processes that caused the observed variabilities in O₃ and CO.
Before evaluating the specific chemical species, variations in the meteorological parameters simulated by the model
are briefly evaluated. Figure 8 compares WRF-Chem simulations with the in situ measurements of meteorological
parameters along the cruise track. Overall, WRF-Chem reproduces these meteorological parameters with only small
295 mean biases, such as -2.3 hPa in pressure, -0.5° C in temperature, and -1.4% in relative humidity (Table 3).
However, model shows limitations in capturing some of the sharp reductions in air temperature and associated
enhancements in relative humidity.

Figure 9 compares WRF-Chem-simulated O₃ and CO with in situ measurements taken along the cruise track. WRF-
Chem is found to reproduce the observed variations in O₃ and CO over the BoB during the summer monsoon season
300 with an overestimation of absolute O₃ levels by 6.2 nmol mol⁻¹ (i.e. ~21% of averaged O₃ value, 29.7 nmol mol⁻¹)
and absolute CO levels by 22 nmol mol⁻¹ (i.e. ~23% of averaged CO value, 96 nmol mol⁻¹). It should be noted here
that the average CO mixing ratio of 96 nmol mol⁻¹ is slightly higher than its actual value, as data points below the
detection limit of the instrument are discarded. Biases in the model simulations can be attributed to the uncertainties
in the simulated meteorology and input emissions; however, in the present study, we use the model fields mainly to
305 investigate temporal variations. The squared correlation coefficients between daily averaged in situ measured and
simulated O₃ and CO are 0.67 and 0.19, respectively. The higher value of the squared correlation coefficient for O₃
demonstrates WRF-Chem's ability to reproduce the observed broad features in surface O₃ over the BoB. Note that
the sharp reductions that caused very low ozone during rainfall episodes are not captured by WRF-Chem, except
during the event of August 10–11, 2009. This will be discussed in detail in Section 5.4.

310

5.3 Diurnal variation

Figure 10 shows the mean delta-diurnal variation, that is the mean value subtracted from the mean diurnal pattern, in
surface O₃ from observations and model simulations for the location where the ship was kept stationary (89° E, 19°
N) for a period of about 15 days. Ozone at each hour shown here is an average of 10 to 15 observations. Ship
315 exhaust contaminated the observations for a period of time between 5 to 14 hours long; data corresponding to this
period is therefore discarded from analysis, leading to a gap. Both the WRF-Chem model and observations showed
only small variability from mean values (delta ozone = -2 to +2 nmol mol⁻¹) during the summer monsoon season.
Neither our limited measurements nor the simulations exhibited any tendency towards net photochemical build-up in
ozone after sunrise during the monsoon. The observations available during 5 to 14 hours on July 23 and 24, 2009
320 also do not show any daytime build up. A net daytime photochemical build up has been reported over the BoB
during both pre-monsoon (Nair et al., 2011) and post-monsoon season (Mallik et al., 2013), as shown for
comparison in Figure 10. The absence of net day-time photochemical build-up and the highly correlated variability
of ozone with residence time over the Indian region (Section 5.1) suggest that spatio-temporal variations in surface
ozone over the BoB during monsoon season are associated with the direct transport, supplemented with en route
325 photochemistry. Note that, due to the insufficient number of observations, diurnal variations in CO and CH₄ are not
discussed.



5.4 Ozone variations during rainfall events

330 An interesting phenomenon observed during the CTCZ experiment is the abrupt reduction in ozone mixing ratios that accompanied the onset of heavy rainfall, despite the low solubility of ozone in water. In this section we investigate the possible causes of these low-ozone events during rainfall over the BoB.

Figure 11 shows variations in O_3 (black circles), TRMM-retrieved rainfall (thick grey vertical bars), and WRF-Chem-simulated vertical winds at pressure levels ranging from 950–750 hPa (coloured bars) during four such events on July 21, 26, and 28–29 and on August 10–11, 2009. As high time-resolution in situ measurements of rainfall were 335 not available aboard ship, Figure 11 therefore uses 3-hourly rainfall retrievals from the TRMM, co-located with ozone measurements. During these events, CO mixing ratios also show a reduction of about $\sim 56 \text{ nmol mol}^{-1}$, with observed values falling below the detection limit of the instrument during the first event of July 21, 2009 (not shown). Although CO measurements are not available for the second and third event, during the fourth event (August 10–11, 2009) CO mixing ratios showed an enhancement due to transport from strong source regions (see 340 Section 5.1). While the first three low- O_3 events are not captured by WRF-Chem (Fig 9a), the fourth event is reproduced.

Wet scavenging does not directly reduce ozone, as its water solubility is low; as a result, some dynamic process could be responsible for the observed reductions in ozone during rainfall. Airmasses could undergo downdrafts during heavy rainfall (Kumar et al., 2005) through air drag by the falling rain drops and in mesoscale subsidence that 345 compensates convective updrafts. We suggest that, in the presence of ozone-poor airmass aloft, a downdraft would result in reductions in surface ozone mixing ratios. The model-simulated meteorology shows occurrences of downdrafts at different pressure levels during the first three events on July 21, 26, and 28–29 (Fig. 11a–c), which we further corroborate with measurements of air temperature aboard. Downdrafts of free tropospheric air could lead to a reduction in near-surface temperature by as much as $10 \text{ }^\circ\text{C}$ within a few minutes (Ahrens, 2009). Air temperature 350 measured aboard ship showed a sharp decrease of $2\text{--}4 \text{ }^\circ\text{C}$, coinciding with the first three low-ozone events (Fig. 12). The reductions in temperature caused by downdrafts are generally short-lived (Ahrens, 2009), it is confirmed in the case of these events (Fig. 12).

Model-simulated vertical winds and variations in air temperature suggest that downdrafts did occur during the first three rainfall events. As in situ measurements of ozone vertical profiles are not available over the BoB during the 355 summer monsoon season, we instead used observations taken at Thumba, Thiruvananthapuram, in the southern Indian region as a case study to investigate this hypothesis. For general details of the typical diurnal and seasonal variations in O_3 at Thumba, please see Nair et al. (2002), David and Nair (2011), and Girach et al. (2012). Figure 13a shows the temporal variation in surface O_3 on July 15, 2011 at Thumba, along with 5-minute accumulated rainfall. Here, surface ozone is observed to decline from 25 to 13 nmol mol^{-1} within $15\text{--}20$ minutes, coinciding with the occurrence of intense rainfall ($3.5\text{--}0.5 \text{ mm}$ rain over a period of 5 minutes). Measurements of the O_3 vertical 360 profile are not available for this day due to the rainy conditions; a profile measured on July 28, 2011 is therefore shown in Fig. 13b. This profile has significantly lower ozone mixing ratios aloft ($\sim 22 \text{ nmol mol}^{-1}$ at $\sim 1 \text{ km}$) than near surface ($\sim 42 \text{ nmol mol}^{-1}$). A typical mixed layer height is about $0.6 \pm 0.2 \text{ km}$ over Thumba, Thiruvananthapuram



(Nair et al., 2011) during the summer monsoon season; above this height, O₃ mixing ratios sharply decrease with
365 altitude. The present case study suggests the presence of ozone-poor airmasses aloft than those near the surface over
the south Indian region during summer monsoon. With an ozone distribution as observed in the present case study at
Thumba, the downdraft during intense rainfall could lead to the mixing of free-tropospheric air with near-surface air,
or to the replacement of surface air with free-tropospheric ozone-poor air.

Although air temperature measurements could not be made during the fourth event (10–11 August 2009) due to a
370 technical problem, model meteorology does not indicate a downdraft during this event (Fig. 11d), indicating the
dominance of a different process. As WRF-Chem-simulated ozone variability is in good agreement with
observations during this event, we used various tendency terms from WRF-Chem to investigate the relative
influences of different processes. The variations in instantaneous values for horizontal advection tendency, vertical
advection tendency, and net tendency (i.e. the sum of chemical, vertical mixing, convective, vertical advection, and
375 horizontal advection), along with modelled O₃ over the two locations during the event are shown in Figure 14. The
tendency values shown here are derived by subtracting the accumulated tendencies at (n-1)th hour from the
accumulated tendency at nth hour. The vertical dotted lines show the time of a low-ozone event.

Both the horizontal and net tendencies (Fig. 14b,e) show negative values, indicating that they are contributing
towards a reduction in ozone mixing ratios (Fig. 14a,d). However, as the time of the event approaches, it is the
380 horizontal advection tendency term that is significantly negative (Fig. 14c, f), while other terms are small and close
to zero. Horizontal advection is therefore suggested to dominate during the low-ozone event of August 10–11, 2009.
The influence of horizontal advection on O₃ during this event is shown more clearly in Fig. 15, which shows the
spatial distribution of O₃ and CO from WRF-Chem before the event (16:00 and 19:00 UT) and during the event
(22:00 UT) on August 10, 2009. The white triangles show the two locations where the event was observed. During
385 16:00 and 19:00 UT, a patch of high ozone mixing ratios (45 nmol mol⁻¹ and higher) is seen to be distributed over a
large region surrounding the measurement location. This large patch of elevated ozone mixing ratios is horizontally
advected eastward from 16:00 to 19:00 and then towards 22:00 UT (event time). As a result of this rapid advection,
the high-ozone airmasses are transported from the coastal regions to deeper into the BoB; by the time they reached
the location of observation, ozone mixing ratios are observed to be lower (25–35 nmol mol⁻¹) during the event time
390 (22:00 UT). A patch of higher levels of CO (~300 nmol mol⁻¹) was also found to be distributed across the east coast
of the Indian region. Transport and dilution of this CO patch is, however, less pronounced than the high-ozone
airmasses, possibly due to the relatively longer lifetime of CO. Thus, we suggest that the horizontal advection
played a key role in transporting O₃-rich airmasses deeper into the BoB region, while it diluted O₃ levels near the
coastal regions in southern India during the fourth event.

395

5.5 Seasonal variation in trace gases over the BoB

In this section, we combine the first monsoon-time measurements of ozone taken in the present study, with data
from previous campaigns (see Table 3) to investigate the seasonal variation in ozone over the BoB (Fig. 16). O₃,
CO, and CH₄ mixing ratios are averaged over northern and central BoB regions, as defined in Fig. 3.



400 Overall, higher O_3 mixing ratios are present over both northern and central BoB during the winter, while significantly lower O_3 levels are observed during the spring–summer (with more scatter in the data over central BoB). The O_3 seasonal amplitude (i.e., the range from maxima to minima) is estimated to be $\sim 39 \text{ nmol mol}^{-1}$ over northern BoB and $\sim 27 \text{ nmol mol}^{-1}$ over central BoB. The monsoonal surface ozone mixing ratios ($\sim 30 \pm 7 \text{ nmol mol}^{-1}$) are nearly half those observed during winter ($63 \pm 5 \text{ nmol mol}^{-1}$) over northern BoB. During December 2008–
405 January 2009, February 2003, March 2006, and November 2010, the ozone mixing ratios were significantly higher (by ~ 3 – 22 nmol mol^{-1}) over northern BoB than those over central BoB. However, over the course of February 2001, ozone mixing ratios were higher over central BoB ($\sim 38 \text{ nmol mol}^{-1}$) than that over northern BoB ($\sim 14 \text{ nmol mol}^{-1}$). In contrast, during summer monsoon season, average ozone mixing ratios are comparable or only slightly higher over northern BoB ($30 \pm 7 \text{ nmol mol}^{-1}$) as compared to that over central BoB ($27 \pm 5 \text{ nmol mol}^{-1}$).

410 As compared with the summer monsoon season, when CO mixing ratios were lower, over northern BoB, CO mixing ratios were higher during the winter, while over central BoB, CO mixing ratios were higher during the pre-monsoon season. For O_3 , spring–summer had the lower mixing ratios in both regions. The seasonal amplitude in CO mixing ratios is estimated to be $\sim 205 \text{ nmol mol}^{-1}$ over northern BoB and $\sim 124 \text{ nmol mol}^{-1}$ over central BoB. The monsoonal CO mixing ratio ($\sim 95 \text{ nmol mol}^{-1}$) is about one third that of the winter season ($302 \text{ nmol mol}^{-1}$) over northern BoB.
415 During the present study, average CO mixing ratios were comparable over northern ($95 \pm 25 \text{ nmol mol}^{-1}$) and central BoB ($101 \pm 27 \text{ nmol mol}^{-1}$).

A clear inference about seasonal patterns is difficult in the case of CH_4 , however a tendency of lower levels towards winter can be seen. Higher mixing ratios ~ 1.95 (~ 1.91) $\mu\text{mol mol}^{-1}$ were observed during November 2010 over northern BoB, and during February–March 2001 over central BoB, as compared to those from other studies. In the
420 present study, average mixing ratios of methane are significantly higher over northern BoB ($1.86 \pm 0.12 \mu\text{mol mol}^{-1}$) as compared to over central BoB ($1.72 \pm 0.14 \mu\text{mol mol}^{-1}$) during the summer monsoon season. The higher tropospheric CH_4 that has been observed over the central and northern Indian landmass during the summer monsoon season (Kavitha and Nair, 2016) could be responsible for the higher CH_4 that is observed over northern BoB in the present study. Owing to the longer lifetime of CH_4 , diffusion of CH_4 from a hotspot region over the eastern IGP to
425 northern BoB might be the other source of higher CH_4 levels over northern BoB during summer monsoon season. An analysis of an emission inventory by sector over the hotspot region (i.e. eastern IGP) indicates that these higher methane emissions are due to rice cultivation, waste treatment and livestock. The surface CH_4 observations obtained during the present study show the highest variability (i.e. the difference between maxima and minima) when compared to earlier studies: $0.53 \mu\text{mol mol}^{-1}$ over northern BoB and $0.39 \mu\text{mol mol}^{-1}$ over central BoB. We attribute
430 this high variability to the relative source strengths over central and northern India as compared to southern India, highlighting the regional differences in CH_4 variability across India (Kavitha and Nair, 2016).

Seasonal variations in trace gases over the BoB are attributed to seasonal changes in the meteorological conditions, emissions, and photochemistry over the South Asian region, as well as to synoptic scale transport patterns. Wintertime stronger westerly winds transport the pollution from South Asia including that of the Indo-Gangetic
435 basin to the BoB region. Monsoonal circulation, in contrast, carries cleaner marine airmasses to the BoB from the oceanic regions. However, as observed during the CTCZ, polluted continental or coastal airmasses can also



occasionally be transported deeper over the BoB. Intense monsoonal rainfall generally leads to wet removal of ozone precursors, while cloudy and rainy meteorological conditions suppress ozone formation. Along with the importance of monsoonal convection in cloud formation, rainfall, and uplifting the boundary layer pollution, rapid horizontal advection is also an important process during the summer monsoon, especially affecting the near-surface variability of trace gases over the oceanic regions adjacent to India.

6. Conclusions

In this paper, we presented the ship-borne in situ measurements of O_3 , CO, and CH_4 that were carried out as a part of the CTCZ experiment over the BoB during July–August 2009, the first time that such measurements had been taken over this region during the summer monsoon season. We analyzed the spatial and temporal variations in our observations and compared them with simulations from a regional chemistry transport model (WRF-Chem), as well as with observations from previous campaigns over the BoB. The main conclusions from the study are:

1. These first monsoonal observations of O_3 , CO, and CH_4 show significant spatio-temporal variability over the BoB, with mixing ratios varying in the range of 8–54 (mean: 29.7 ± 6.8) $nmol\ mol^{-1}$, 50–200 (mean: 96 ± 25) $nmol\ mol^{-1}$, and 1.57–2.15 (mean: 1.83 ± 0.14) $\mu mol\ mol^{-1}$, respectively. The O_3 , CO, and CH_4 mixing ratios are slightly higher or comparable (O_3 : 30 ± 7 $nmol\ mol^{-1}$, CO: 95 ± 25 $nmol\ mol^{-1}$, CH_4 : 1.86 ± 0.12 $\mu mol\ mol^{-1}$) over northern BoB as compared to over central BoB (O_3 : 27 ± 5 $nmol\ mol^{-1}$, CO: 101 ± 27 $nmol\ mol^{-1}$, CH_4 : 1.72 ± 0.14 $\mu mol\ mol^{-1}$). The difference (~ 0.14 $\mu mol\ mol^{-1}$) between CH_4 mixing ratios over northern and central BoB is most significant.
2. Back-trajectory analysis shows effects of long-range transport from northern or central India to northern BoB, and from southern India to central BoB. The correlated variations of O_3 mixing ratio and percentage residence time of air parcels over the Indian regions suggest that the enrichment of ozone and precursors in air parcels over the BoB is associated with both emissions and photochemistry over the Indian region. The trajectory analysis and mean diurnal variations show that the observed variation in surface O_3 is primarily due to transport and en route photochemistry, rather than to local photochemical production over the BoB during monsoon season.
3. The observed spatio-temporal variations in surface O_3 and CO during summer monsoon season are generally reproduced by the WRF-Chem model, although the absolute mixing ratios of O_3 and CO are typically overestimated by about 20%.
4. We observed four low-ozone events coinciding with intense rainfall over the BoB. After analysing the observed variability in air temperature, model simulations of vertical winds, and an ozone-profile case study from southern India, we suggest that first three low-ozone events were due to strong downdrafts of ozone-poor airmasses. Analysis of the fourth low-ozone event, which is successfully reproduced by the model, shows the pivotal role of horizontal advection in transporting ozone-rich airmasses deeper over the BoB.
5. Finally, we combined our monsoon time measurements with previous campaigns over the BoB during other seasons to investigate the seasonal variability in trace gases over the BoB. O_3 and CO are shown to have pronounced seasonality, O_3 having amplitudes of about 39 and 27 $nmol\ mol^{-1}$, and CO having amplitudes of about 207 and 124 $nmol\ mol^{-1}$ over northern and central BoB, respectively.



Our study fills a gap of experimental data during the summer monsoon over the BoB, providing information on the extent of seasonal variability. We recommend supplementing these findings with ship-borne experiments featuring collocated vertical profile observations from balloon-borne and aircraft-based platforms over the oceanic regions surrounding India to better understand the role of both large-scale dynamics (e.g. Ojha et al., 2016) and of regional influences due to South Asian outflow (see Lawrence and Lelieveld, 2010, and references therein). Such a future study would also improve our understanding of the changes that take place in the atmospheric oxidation capacity during the summer monsoon season.

Acknowledgements

We thank all of the CTCZ and ICRP organizers for providing the opportunity to participate in the 2009 CTCZ experiment. We are thankful to the Director of the National Centre for Antarctic and Ocean Research (NCAOR), Goa for providing ship-board facilities. We gratefully acknowledge Prof. G. S. Bhatt (Indian Institute of Science, Bengaluru, India) and his team for providing the measurements of meteorological parameters onboard ship. We also thank the chief scientist on board *SagarKanya* for providing necessary support during the cruise. The authors gratefully acknowledge the NOAA Air Resources Laboratory (ARL) for the providing the HYSPLIT transport and dispersion model and READY website (<http://www.arl.noaa.gov/ready.php>) used in this publication. The rainfall estimations (3B42) from the TRMM satellite were obtained from the NASA/GSFC via their website <http://mirador.gsfc.nasa.gov/>. Use of INTEX-B and HTAP (http://edgar.jrc.ec.europa.eu/htap_v2/index.php?SECURE=123) anthropogenic emissions is gratefully acknowledged. Initial and boundary-conditions data for meteorological fields were used from the ERA interim of ECMWF. Use of MOZART-4/GEOS5 initial and boundary conditions data for chemical fields is acknowledged. Data/processors for anthropogenic emissions, biogenic emissions, and biomass burning obtained from NCAR ACD website are gratefully acknowledged. The authors acknowledge the use of MPG supercomputer HYDRA (<http://www.mpcdf.mpg.de/services/computing/hydra>) for model simulations.

References

- Ackermann, I. J., Hass, H., Memmesheimer, M., Ebel, A., Binkowski, F. S., and Shankar, U.: Modal aerosol dynamics model for Europe: development and first applications, *Atmos. Environ.*, 32, 2981–2999, 1998.
- Ahrens C. D.: *Meteorology Today- an introduction to weather, climate, and the environment*, Brooks/Cole, USA, 2009.
- Ansari, T. U., Ojha, N., Chandrasekar, R., Balaji, C., Singh, N., Gunthe, S. S., Competing impact of anthropogenic emissions and meteorology on the distribution of trace gases over Indian region, *J. Atmos. Chem.*, doi:10.1007/s10874-016-9331-y, pp. 1-18, 2016.



- Bennet, C. and Engardt, M.: A regional model for surface ozone in Southeast Asia. *Tellus B*, 60: 718–728. doi: 10.1111/j.1600-0889.2008.00378.x, 2008.
- 510 Bergamaschi, P., Hein, R., Heimann, M., and Crutzen, P. J.: Inverse modeling of the global CO cycle: 1. Inversion of CO mixing ratios, *J. Geophys. Res.-Atmos.*, 105, 1909–1927, doi:10.1029/1999JD900818, 2000.
- Binkowski, F. S. and Shankar, U.: The regional particulate matter model: 1. Model description and preliminary results, *J. Geophys. Res.*, 100, 26191–26209, doi:10.1029/95JD02093, 1995.
- Brasseur, G.P., Orlando, J.J., and Tyndall, G.S.: *Atmospheric Chemistry and Global Change*. Oxford University Press, New York, pp. 209-234, 1999.
- 515 Chen, F. and Dudhia, J.: Coupling and advanced land surface-hydrology model with the Penn State-NCAR MM5 modeling system, Part I: Model implementation and sensitivity, *Mon. Weather Rev.*, 129, 569–585, 2001.
- Chou, M.-D. and Suarez, M. J.: An efficient thermal infrared radiation parametrization for use in general circulation models, *NASA Tech. Memo.*, 104606, 85 pp., 1994.
- 520 Cooper, O. R., Parrish, D. D., Ziemke, J., Balashov, N. V., Cupeiro, M., Galbally, I. E., Gilge, S., Horowitz, L. , Jensen, N. R., Lamarque, J.-F., Naik, V., Oltmans, S. J., Schwab, J., Shindell, D. T., Thompson, A. M., Thouret, V., Wang, Y., and Zbinden, R. M.: Global distribution and trends of tropospheric ozone: An observation-based review, *Elementa: Science of the Anthropocene*, 2: 000029, doi: 10.12952/journal.elementa.000029, 2014.
- 525 Crutzen, P.J., Lawrence, M.G., and Poschl, U.: On the background photochemistry of tropospheric ozone. *Tellus* 51A, 123-146, 1999.
- David, L. M. and Nair, P. R.: Diurnal and seasonal variability of surface ozone and NO_x at a tropical coastal site: Association with mesoscale and synoptic meteorological conditions, *J. Geophys. Res.*, 116, D10303, doi:10.1029/2010JD015076, 2011.
- 530 David, L.M., Girach, I. A., Nair, P.R.: Distribution of ozone and its precursors over Bay of Bengal during winter 2009: role of meteorology, *Ann. Geophys.*, 29, 1613–1627, doi:10.5194/angeo-29-1613-2011, 2011.
- Draxler, R.R. and Rolph, G.D.: HYSPLIT (HYbrid Single-Particle Lagrangian Integrated Trajectory) Model access via NOAA ARL READY Website (<http://www.arl.noaa.gov/HYSPLIT.php>), NOAA Air Resources Laboratory, Silver Spring, MD.
- 535 Finlayson-Pitts, B.J., Pitts Jr., J.N., 2000. *Chemistry of the Upper and Lower Atmosphere: Theory, Experiments, and Applications*. Academic Press, USA, 2003.



- Fishman, J., Solomon, S., and Crutzen, P. J.: Observational and theoretical evidence in support of a significant in situ photochemical source of tropospheric ozone, *Tellus*, 31, 432–446, 1979.
- Fung, I., John, J., Lerner, J., Matthews, E., Prather, M., Steele, L. P., and Fraser, P. J.: Three-dimensional model synthesis of the global methane cycle, *J. Geophys. Res.* 96, 13033–13065, 1991.
- 540 Girach, I.A. and Nair, P.R.: Spatial distribution of near-surface CO over bay of Bengal during winter: role of transport. *J. Atmos. Solar Terr. Phys.*, 72, 1241–1250, doi:10.1016/j.jastp.2010.07.02, 2010.
- Girach, I. A., P. R. Nair, L. M. David, P. Hegde, M. K. Mishra, G. M. Kumar, S. M. Das, N. Ojha, and Naja M.: The changes in near-surface ozone and precursors at two nearby tropical sites during annular solar eclipse of 15 January 2010, *J. Geophys. Res.*, 117, D01303, doi:10.1029/2011JD016521, 2012.
- 545 Grell, G. A., Peckham, S. E., Schmitz, R., McKeen, S. A., Frost, G., Skamarock, W. C., and Eder, B.: Fully coupled “online” chemistry within the WRF model, *Atmos. Environ.*, 39, 6957–6975, 2005.
- Guenther, A., Karl, T., Harley, P., Wiedinmyer, C., Palmer, P. I., and Geron, C.: Estimates of global terrestrial isoprene emissions using MEGAN (Model of Emissions of Gases and Aerosols from Nature), *Atmos. Chem. Phys.*, 6, 3181–3210, doi:10.5194/acp-6-3181-2006, 2006.
- 550 Heagle, A.S.: Ozone and crop yield. *Annual Review of Phytopathology* 27, 397–423, 1989.
- Huffman, G.J., Adler, R.F., Rudolf, B., Schneider, U., and Keehn, P.R.: Global precipitation estimates based on a technique for combining satellite-based estimates, rain gauge analysis, and NWP model precipitation information. *J. Clim.* 8, 1284–1295, doi: 10.1175/1520-0442(1995)008<1284:GPEBOA>2.0.CO;2, 1995.
- IPCC-AR5, Fifth Assessment Report of the Intergovernmental Panel on Climate Change, 2013.
- 555 Jacob, D.: Introduction to Atmospheric Chemistry, Princeton University Press, 1999.
- Janjic, Z. I.: The surface layer in the NCEP Eta Model, Eleventh Conference on Numerical Weather Prediction, Norfolk, VA, 19–23 August, Amer. Meteor. Soc., Boston, Boston, MA, 354–355, 1996.
- Janjic, Z. I.: Nonsingular Implementation of the Mellor–Yamada Level 2.5 Scheme in the NCEP Meso Model, NCEP office Note, 437, 61 pp., 2002.
- 560 Janssens-Maenhout, G., Crippa, M., Guizzardi, D., Dentener, F., Muntean, M., Pouliot, G., Keating, T., Zhang, Q., Kurokawa, J., Wankmuller, R., Denier van der Gon, H., Klimont, Z., Frost, G., Darras, S. and Koffi, B.: HTAP_v2: a mosaic of regional and global emission gridmaps for 2008 and 2010 to study hemispheric transport of air pollution, *Atmos. Chem. Phys. Discuss.*, 15, 12867–12909, doi:10.5194/acpd-15-12867-2015, 2015.



- 565 Kavitha, M. and Nair P. R.: Region-dependent seasonal pattern of methane over Indian region as observed by SCIAMACHY, *Atmospheric Environment* 131, 316-325, doi: 10.1016/j.atmosenv.2016.02.008, 2016.
- Komhyr, W.D.: Electrochemical concentration cells for gas analysis. *Ann. Geophys.* 25, 203-210, 1969.
- Komhyr, W.D., Barnes, R.A., Brothers, G.B., Lathrop, J.A., and Opperman, D.P.: Electrochemical concentration cell ozonesonde performance evaluation during STOIC 1989. *J. Geophys. Res.* 100 (D5), 9231-9244, doi: 570 10.1029/94JD02175, 1995.
- Kumar K. K., Jain A. R., and Rao D. N.: VHF/UHF radar observations of tropical mesoscale convective systems over southern India, *Annales Geophysicae*, 23, 1673-1683, 1432-0576/ag/2005-23-1673, 2005.
- Kumar, R., M. Naja, G. G. Pfister, M. C. Barth, and Brasseur, G. P.: Simulations over South Asia using the Weather Research and Forecasting model with Chemistry (WRF-Chem): set-up and meteorological evaluation, 575 *Geosci. Model. Dev.*, 5, 321-343, doi:10.5194/gmd-5-321-2012, 2012a.
- Kumar, R., Naja, M., Pfister, G. G., Barth, M. C., Wiedinmyer, C., and Brasseur, G. P.: Simulations over South Asia using the Weather Research and Forecasting model with Chemistry (WRFChem): chemistry evaluation and initial results, *Geosci. Model Dev.*, 5, 619-648, doi:10.5194/gmd-5-619-2012, 2012b.
- Kumar, R., M. C. Barth, G. G. Pfister, V. S. Nair, S. D. Ghude, and Ojha N.: What controls the seasonal cycle of 580 black carbon aerosols in India?, *J. Geophys. Res. Atmos.*, 120, doi:10.1002/2015JD023298, 2015.
- Lal, S., Chand, D., Sahu, L.K., Venkataramani, S., Brasseur, G., Schultz, M.G.: High levels of ozone and related gases over the Bay of Bengal during winter and early spring of 2001, *Atmos. Environ.* 40, 1633-1644, 2006.
- Lal, S. and Lawrence, M.G.: Elevated mixing ratios of surface ozone over the Arabian Sea. *Geophysical Research Letters* 28, 1487-1490, 2001. 585
- Lal, S., Sahu, L.K., and Venkataramani, S.: Impact of transport from the surrounding continental regions on the distributions of ozone and related trace gases over the Bay of Bengal during February 2003. *J. Geophys. Res.* 112, D14302, doi:10.1029/2006JD008023, 2007.
- Lawrence, M. G., and J. Lelieveld: Atmospheric pollutant outflow from southern Asia: a review, *Atmos. Chem. Phys.*, 10, 11017-11096, doi:10.5194/acp-10-11017-2010, 2010. 590
- Lelieveld, J., and F.J. Dentener: What controls tropospheric ozone? *J. Geophys. Res.*, 105, 3531-3551, doi:10.1029/1999JD901011, 2000.
- Lelieveld, J., P. J. Crutzen, V. Ramanathan, M. O. Andreae, C. A. M. Brenninkmeijer, T. Campos, G. R. Cass, R. R. Dickerson, H. Fischer, J. A. de Gouw, A. Hansel, A. Jefferson, D. Kley, A. T. J. de Laat, S. Lal, M. G.



- 595 Lawrence, J. M. Lobert, O. L. Mayol-Bracero, A. P. Mitra, T. Novakov, S. J. Oltmans, K. A. Prather, T. Reiner, H. Rodhe, H. A. Scheeren, D. Sikka, and J. Williams: The Indian Ocean experiment: Widespread air pollution from South and Southeast Asia, *Science*, 291, 1031–1036, 2001.
- Lelieveld, J., H. Berresheim, S. Borrmann, P. J. Crutzen, F. J. Dentener, H. Fischer, J. Feichter, P. J. Flatau, J. Heland, R. Holzinger, R. Kormann, M. G. Lawrence, Z. Levin, K. M. Markowicz, N. Mihalopoulos, A. Minikin, V. Ramanathan, M. de Reus, G. J. Roelofs, H. A. Scheeren, J. Sciare, H. Schlager, M. Schultz, P. Siegmund, B. Steil, E. G. Stephanou, P. Stier, M. Traub, C. Warneke, J. Williams, H. Ziereis, *Science*, vol 600 298, issue 5594, pp. 794–799, doi: 10.1126/science.1075457, 2002.
- Lin, Yuh–Lang, Richard D. Farley, and Harold D. Orville, 1983: Bulk Parameterization of the Snow Field in a Cloud Model. *J. Climate Appl. Met.*, **22**, 1065–1092.
- 605 Mahapatra, P.S., Panda, S., Walvekar, P.P., Kumar, R., Das, T., and Gurjar, B.R.: Seasonal trends, meteorological impacts, and associated health risks with atmospheric concentrations of gaseous pollutants at an Indian coastal city. *Environ Sci Pollut Res*, doi: 10.1007/s11356-014-3078-2, 2014.
- Mallik, C., Lal, S., Venkataramani, S., Naja, M., and Ojha, N.: Variability in ozone and its precursors over the Bay of Bengal during post monsoon: Transport and emission effects. *J. Geophys. Res. Atmos.*, 118, 610 doi:10.1002/jgrd.50764, 2013.
- Mlawer, E. J., Taubman, S. J., Brown, P. D., Iacono, M. J., and Clough, S. A.: Radiative transfer for inhomogeneous atmospheres: RRTM, a validated correlated-k model for the longwave, *J. Geophys. Res.-Atmos.*, 102, 16663–16682, doi:10.1029/97JD00237, 1997.
- Mühle, J., Zahn, A., Brenninkmeijer, C.A.M., Gros, V., and Crutzen, P.J.: Air mass classification during the 615 INDOEX R/V cruise using measurements of non-methane hydrocarbons, CH₄, CO₂, CO, 14CO, and δ¹⁸O(CO). *J. Geophys. Res.* 107(D19), 8021, doi:10.1029/2001JD000730, 2002.
- Monks, P. S., Archibald, A. T., Colette, A., Cooper, O., Coyle, M., Derwent, R., Fowler, D., Granier, C., Law, K. S., Mills, G. E., Stevenson, D. S., Tarasova, O., Thouret, V., von Schneidemesser, E., Sommariva, R., Wild, O., and Williams, M. L.: Tropospheric ozone and its precursors from the urban to the global scale from air 620 quality to short-lived climate forcer, *Atmos. Chem. Phys.*, 15, 8889–8973, doi:10.5194/acp-15-8889-2015, 2015.
- Moorthy K. K., V. S. Nair, Babu S. S., and Satheesh S. K.: Spatial and vertical heterogeneities of aerosol radiative forcing over the oceanic regions surrounding the Indian peninsula: climate implications, *Q. J. R. Meteorol. Soc.*, 135, 2131–2145, 2009.



- 625 Nair, P. R., Chand, D., Lal, S., Modh, K. S., Naja, M., Parameswaran, K., Ravindran, S., and Venkataramani, S.: Temporal variations in surface ozone at Thumba (8.6 N, 77 E) –a tropical coastal site in India, *Atmos. Environ.*, 36, 603–610, doi:10.1016/S1352-2310(01)00527-1, 2002.
- Nair, P. R., David, L. M., Girach, I. A., and George, S. K.: Ozone in the marine boundary layer of Bay of Bengal during post-winter period: Spatial pattern and role of meteorology, *Atmos. Environ.*, 45, 4671–4681, 2011.
- 630 Nair, S. K., Anurose, T. J., Subrahmanyam, D. B., Kirankumar, N. V. P., Santosh, M., Sijikumar, S., Mohan, M., and Nambodiri, K. V. S.: Characterization of the Vertical Structure of Coastal Atmospheric Boundary Layer over Thumba (8.5N, 76.9E) during Different Seasons, *Advances in Meteorology*, 390826, doi:10.1155/2011/390826, 2011.
- Nair, V. S., S. K. Satheesh, K. K. Moorthy, S. S. Babu, S. K. George, and Nair P. R.: Surprising observation of large Anthropogenic Aerosol Fraction over the near-pristine Southern Bay of Bengal: Climate Implications, *J. Geophys. Res. Atmos.*, 115, D21201, doi:10.1029/2010JD013954, 2010.
- 635 Naja, M., D. Chand, L. Sahu, and Lal S.: Trace gases over marineregions around India, *Ind. J. Mar. Sci.*, 33(1), 95–106, 2004.
- Ojha, N., M. Naja, K. P. Singh, T. Sarangi, R. Kumar, S. Lal, M. G. Lawrence, T. M. Butler, and Chandola H. C.: Variabilities in ozone at a semi-urban site in the Indo-Gangetic Plain region: Association with the meteorology and regional process, *J. Geophys. Res.*, 117, D20301, doi:10.1029/2012JD017716, 2012.
- Ojha N., M. Naja, T. Sarangi, R. Kumar, P. Bhardwaj, S. Lal, S. Venkataramani, R. Sagar, A. Kumar, Chandol H. C.: On the processes influencing the vertical distribution of ozone over the central Himalayas: Analysis of yearlong ozonesonde observations, *Atmospheric Environment* 88, 201–211, doi:10.1016/j.atmosenv.2014.01.031, 2014.
- 645 Ojha, N., Pozzer, A., Rauthe-Schöch, A., Baker, A. K., Yoon, J., Brenninkmeijer, C. A. M., and Lelieveld, J.: Ozone and carbon monoxide over India during the summer monsoon: regional emissions and transport, *Atmos. Chem. Phys.*, 16, 3013–3032, doi:10.5194/acp-16-3013-2016, 2016.
- Randel, W. J., Park, M., Emmons, L., Kinnison, D., Bernath, P., Walker, K. A., Boone, C., and Pumphrey H.: Asian monsoon transport of pollution to the stratosphere, *Science*, 328, 611–613, 2010.
- 650 Ravikumar K., Tiwari Y. K., Valsala V., and Murtugudde R.: On understanding of land-ocean CO₂ contrast over Bay of Bengal: A case study during 2009 summer monsoon, *Environmental Science and Pollution Research*, 21–7, 5066–5075, DOI: 10.1007/s11356-013-2386-2, 2014.
- Rolph, G. D.: Real-time Environmental Applications and Display sYstem (READY) Website (<http://www.arl.noaa.gov/ready.php>), NOAA Air Resources Laboratory, Silver Spring, MD., 2003.
- 655



- Sahu, L.K., Lal, S., and Venkataramani, S.: Distributions of O₃, CO and hydrocarbons over the Bay of Bengal: a study to assess the role of transport from southern India and marine regions during September-October 2002. *Atmos. Environ.* 40, 4633-4645, 2006.
- 660 Sahu, L. K., and Lal, S.: Changes in surface ozone levels due to convective downdrafts over the Bay of Bengal, *Geophys. Res. Lett.*, 33, L10807, doi:10.1029/2006GL025994, 2006.
- Sawa, Y., et al.: Widespread pollution events of carbon monoxide observed over the western North Pacific during the East Asian Regional Experiment (EAREX) 2005 campaign, *J. Geophys. Res.*, 112, D22S26, doi:10.1029/2006JD008055, 2007.
- 665 Scheeren, H. A., Lelieveld, J., Roelofs, G. J., Williams, J., Fischer, H., de Reus, M., de Gouw, J. A., Warneke, C., Holzinger, R., Schlager, H., Klüpfel, T., Bolder, M., van der Veen, C., and Lawrence, M.: The impact of monsoon outflow from India and Southeast Asia in the upper troposphere over the eastern Mediterranean, *Atmos. Chem. Phys.*, 3, 1589-1608, doi:10.5194/acp-3-1589-2003, 2003.
- Schell, B., Ackermann, I. J., Hass, H., Binkowski, F. S., and Ebel, A.: Modeling the formation of secondary organic aerosol within a comprehensive air quality model system, *J. Geophys. Res.*, 106, 28275-28293, 2001.
- 670 Seinfeld, J.H., and Pandis, S.N.: *Atmospheric Chemistry and Physics: from air pollution to climate change*, 2nd ed., Wiley-Interscience publication, USA, 2006.
- Smit, H.G.J., Straeter, W., Johnson, B.J., Oltmans, S., Davies, J., Tarasick, D.W., Hoegger, B., Stubi, R., Schmidlin, F., Northam, T., Thompson, A.M., Witte, J.C., Boyd, I., Posny, F.: Assessment of the performance of ECC-ozonesondes under quasi-flight conditions in the environmental simulation chamber: insights from the Juelich Ozone Sonde Intercomparison Experiment (JOSIE). *J. Geophys. Res.* 112, D19306. <http://dx.doi.org/10.1029/2006JD007308>, 2007.
- 675 Sprenger, M., Wernli, H., Bourqui, M.: Stratosphere-Troposphere exchange and its relation to potential vorticity streamers and cutoffs near the extratropical tropopause. *Journal of Atmospheric Science* 64, 1587-1604, 2007.
- 680 Srivastava S., S. Lal, S. Venkataramani, S. Gupta, and Acharya Y. B., Vertical distribution of ozone in the lower troposphere over the Bay of Bengal and the Arabian Sea during ICARB-2006: Effects of continental outflow, *J. Geophys. Res.*, 116, D13301, doi:10.1029/2010JD015298, 2011.
- 685 Srivastava, S., S. Lal, S. Venkataramani, S. Gupta, and Sheel V.: Surface distributions of O₃, CO and hydrocarbons over the Bay of Bengal and the Arabian Sea during pre-monsoon season, *Atmos. Environ.*, 47, 459-467, doi:10.1016/j.atmosenv.2011.10.023 2012.



- Stockwell, W. R., P. Middleton, J. S. Chang, and Tang X.: The second generation regional acid deposition model chemical mechanism for regional air quality modeling, *J. Geophys. Res.*, 95(D10), 16343–16367, doi:10.1029/JD095iD10p16343,1990.
- 690 Subrahmanyam D B, T.J. Anurose, N.V.P. Kiran Kumar, Mannil Mohan, P.K. Kunhikrishnan, Sherine Rachel John, S.S. Prijith, and Dutt C.B.S.: Spatial and temporal variabilities in vertical structure of the Marine Atmospheric Boundary Layer over Bay of Bengal during Winter Phase of Integrated Campaign for Aerosols, gases and Radiation Budget, *Atmospheric Research*, Volume 107, 178-185, doi: 10.1016/j.atmosres.2011.12.014, 2012.
- 695 Tanimoto, H., et al.: Direct assessment of international consistency of standards for ground-level ozone: Strategy and implementation toward metrological traceability network in Asia, *J. Environ. Monit.*, 9, 1183– 1193, doi:10.1039/b701230f,2007.
- Tiwari Y. K. and RaviKumar K.: Glass flask air sample analysis through gas chromatography in India: implications for constraining CO₂ surface fluxes, WMO/GAW Report No. 194, WMO/TD-No.1553, April 2011, 2011.
- 700 Verstraeten, W. W., Boersma, K. F., Zörner, J., Allaart, M. A. F., Bowman, K. W., and Worden, J. R.: Validation of six years of TES tropospheric ozone retrievals with ozonesonde measurements: implications for spatial patterns and temporal stability in the bias, *Atmos. Meas. Tech.*, 6, 1413-1423, doi:10.5194/amt-6-1413-2013, 2013.
- World Health Organization, Environmental Health Criteria 213, Carbon monoxide, 1999.
- 705 Wiedinmyer, C., S. K. Akagi, R. J. Yokelson, L. K. Emmons, J. A. Al-Saadi, J. J. Orlando, and Soja, A.J.: The Fire Inventory from NCAR (FINN): a high resolution global model to estimate the emissions from open burning, *Geosci. Model Dev.*, 4, 625–641, doi:10.5194/gmd-4-625-2011, 2011.
- Zhang, Q., D. G. Streets, G. R. Carmichael, K. B. He, H. Huo, A. Kannari, Z. Klimont, I. S. Park, S. Reddy, J. S. Fu, D. Chen, L. Duan, Y. Lei, L. T. Wang, and Yao Z. L.: Asian emissions in 2006 for the NASA INTEX-B mission, *Atmos. Chem. Phys.*, 9, 5131-5153, doi:10.5194/acp-9-5131-2009, 2009.
- 710



Tables

Table 1. The WRF-Chem options used for parameterization of atmospheric processes.

Atmospheric Process	Option used
Cloud microphysics	Lin et al. scheme (Lin et al., 1983)
Longwave radiation	Rapid Radiative Transfer Model (RRTM; Mlawer et al., 1997)
Shortwave radiation	Goddard shortwave scheme (Chou and Suarez, 1994)
Surface Layer	Monin–Obukhov scheme (Janjic, 1996)
Land surface option	Noah Land Surface Model (Chen and Dudhia, 2001)
Urban surface physics	Urban Canopy Model
Planetary boundary layer	Mellor–Yamada–Janjic scheme (Janjic, 2002)
Cumulus parameterization	New Grell scheme (G3)

715



Table 2. A comparison of averaged surface O₃ mixing ratios over various sites.*boundary layer ozone over the Arabian Sea.

Observation site	Longitude (° E)	Latitude (° N)	Observation period during monsoon season	Mean Surface Daytime Ozone	Standard Deviation	Reference
Arabian Sea						
Arabian Sea	69 –76	9 –19	July–August 2002	9	-	Ali et al., 2009
Ahmedabad	72.6	23	July–August 2003–2007	25*	-	Srivastava et al., 2012
Western coast of India						
Thiruvananthapuram	76.9	8.5	August 2009	23	7	Present Study
Thiruvananthapuram	76.9	8.5	June–August 2008	19	6	David and Nair, 2011
Kannur	75.4	11.9	July 2010–2011	11	4	Nishanth et al., 2014
MtAbu (1.6km amsl)	72.7	24.6	August 1993–2000	25	9	Naja et al., 2003
Ahmedabad	72.6	23	July 1991–1995	22	8	Lal et al., 2002
Ahmedabad	72.6	23	August 1991–1995	17	4	Lal et al., 2002
Central India						
Anantpur	77.65	14.62	July 2009	30	2	Reddy et al., 2011
Eastern coast of India						
Bhubaneswar	86.4	20.5	June–August 2011–2012	29	6	Mahapatra et al., 2014
Bay of Bengal						



Bay of Bengal	80.3–90.1	11–21.1	July–August 2009	30	7	Present Study
---------------	-----------	---------	------------------	----	---	---------------

720

Table 3. A comparison of mean values from observations with model-simulated parameters along with the mean bias. The squared correlation coefficients correspond to the linear regression analysis between daily averaged in situ and simulated parameters.

Parameter	Observation	Model (WRF-Chem)	Mean bias	R ²
Pressure (hPa)	1001.3±2.1	999.0±2.4	-2.3	0.93
Temperature (°C)	29.3±0.9	28.8±0.6	-0.5	0.12
Relative Humidity (%)	87.9±4.2	86.5±2.8	-1.4	0.54
O ₃ (nmol mol ⁻¹)	29.7±6.8	35.9±8.3	6.2	0.67
CO (nmol mol ⁻¹)	96±25	118±37	22	0.19

725



Table 4. A comparison of average mixing ratios of surface trace gases measured over northern BoB (81–91° E, 16–21.5° N) and central BoB (80–91° E, 11–16° N) in different seasons as measured during different experiments. The range of mixing ratios (i.e. minima–maxima) is given in the brackets. *CO mixing ratios below the detection limit (i.e. 50 nmol mol⁻¹) are not considered in the analysis.

730

Study period	Name of Experiment	Reference	O ₃ (nmol mol ⁻¹) over northern BoB	O ₃ (nmol mol ⁻¹) over central BoB	CO (nmol mol ⁻¹) over northern BoB	CO (nmol mol ⁻¹) over central BoB	CH ₄ (μmol mol ⁻¹) over northern BoB	CH ₄ (μmol mol ⁻¹) over central BoB
December 2008–January 2009	W_ICARB	David et al., 2011	63.0±4.7 (50.8–73.8)	40.9±6.7 (27.7–63.5)	302±68 (140–450)	188±53 (50–320)	No data	No data
February 2003	BOBEX-II	Lal et al., 2007	~34.1 (15.8–50.4)	~26.8 (13.9–35.0)	~238 (187–292)	~192 (159–224)	~1.77 (1.70–1.85)	~1.73 (1.68–1.77)
February–March 2001	BOBEX-I	Lal et al., 2006	~23.8 (16.1–38.3)	~38.0 (19.4–62.9)	~194 (165–235)	~227 (97–339)	~1.94 (1.89–2.02)	~1.91 (1.74–2.06)
March–April 2006	ICARB	Nair et al., 2011; Srivastava et al., 2012	27.4±2.9 (21.4–32.6)	13.4±4.2 (3.1–24.6)	~189 (157–235)	~132 (96–167)	~1.84 (1.80–1.88)	~1.80 (1.75–1.84)
July–August 2009	CTCZ	Present Study	30.0±6.9 (8.50–54.1)	27.5±5.0 (8.8–40.5)	95±25* (50–198)*	101±27* (50–157)*	1.86±0.12 (1.62–2.15)	1.72±0.14 (1.57–1.96)
September–October 2002	BOBPS	Sahu et al., 2006	~27.3 (17.8–33.8)	~30.6 (22.5–35.2)	~152 (109–179)	~141 (108–211)	~1.79 (1.72–1.86)	~1.73 (1.68–1.80)
November 2010	No name	Mallik et al., 2013	~46.0 (26.7–59.6)	~38.7 (17.8–60.8)	~223 (131–280)	~188 (42–266)	~1.95 (1.85–2.06)	~1.79 (1.67–1.93)



735 Figures

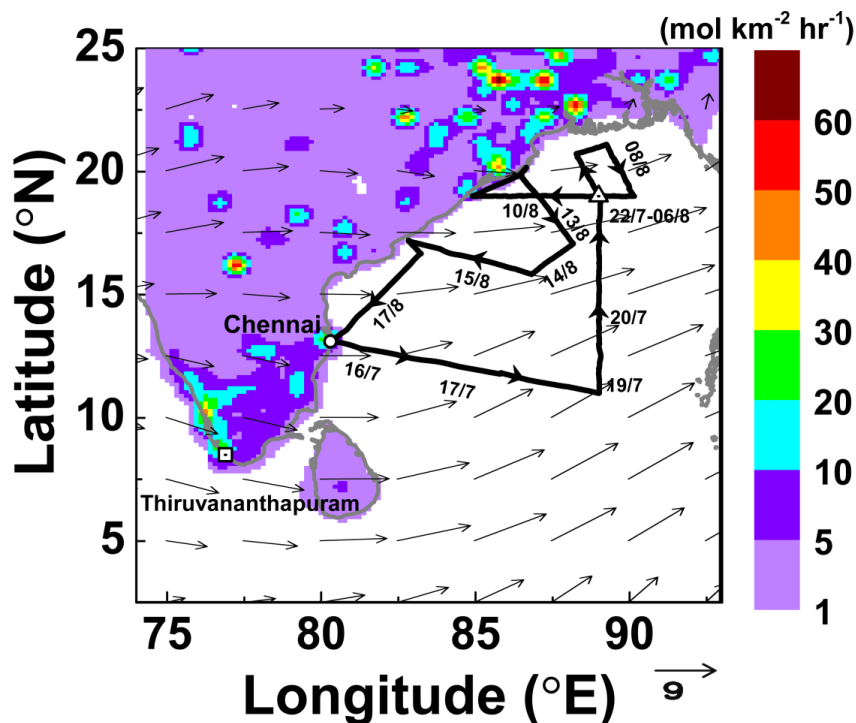
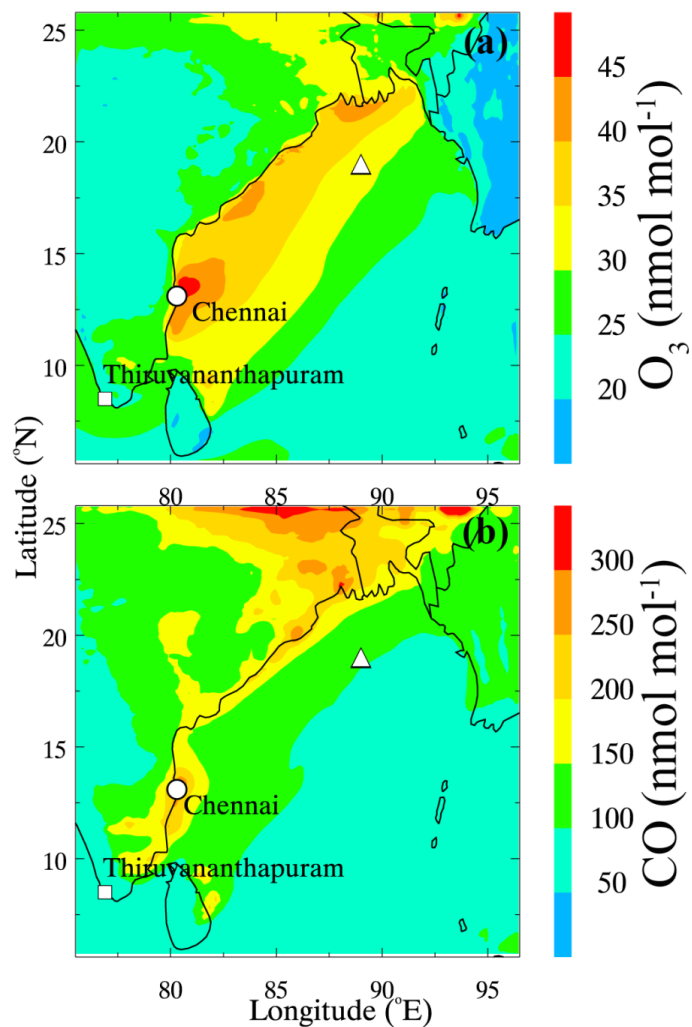


Figure 1. Cruise track (continuous black line) of the Research Vessel *Sagar Kanya* along with synoptic winds at 925 hPa (black thin arrows) averaged over the cruise period. Arrows marked on the track shows the ship direction. The dates corresponding to approximate ship positions are marked along the track. The circle shows the start and end point of the cruise. The square tagged with Thiruvananthapuram shows the location corresponding to the measurements shown in Fig. 15. The location at which the ship was kept stationary (July 22–August 06, 2009) is denoted with a triangle. The background colour map shows the NO_x emissions over the Indian landmass for year 2006 as obtained from the INTEX-B inventory.

740



745

Figure 2. WRF-Chem-simulated spatial distribution of surface O_3 (a) and CO (b) averaged during the July 16–August 17, 2009 period. The location of the ship cruise start and end (Chennai), the ground-based measurement site at Thiruvananthapuram, and the location where the ship was kept stationary are shown by the white circle, square, and triangle, respectively.

750

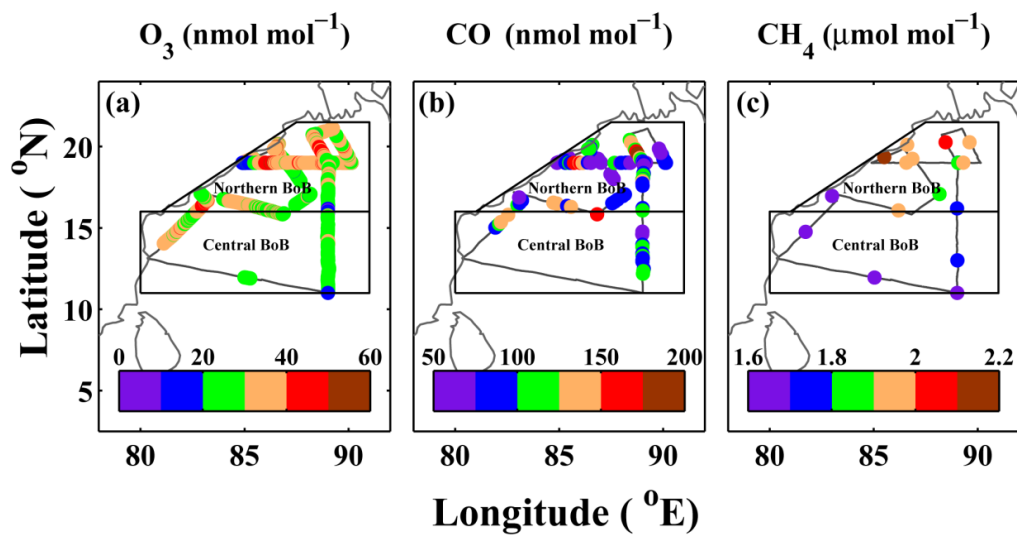


Figure 3. Spatial variation of surface O_3 (a), CO (b), and CH_4 (c) mixing ratios along the cruise track during the CTCZ experiment, which took place during the summer monsoon season. The solid lines demarcate the regions of central and northern BoB.

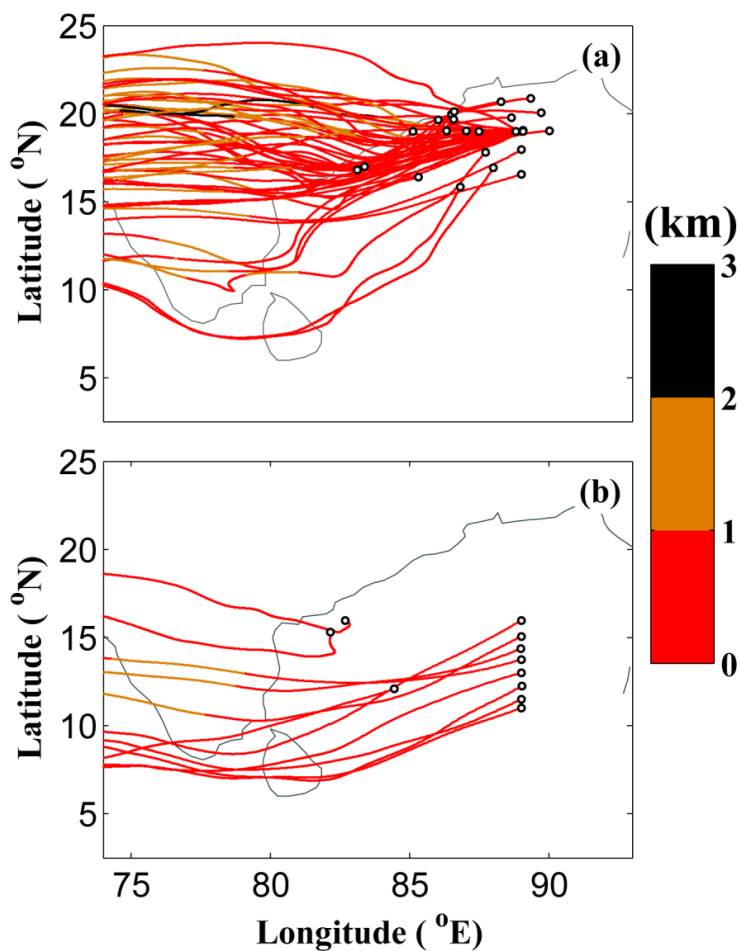


Figure 4. Five-day airmass back-trajectories during the study period ending at the measurement locations (small black circles) grouped for corresponding airmasses over (a) northern BoB and (b) central BoB. The colour scale shows the height (in km) of the trajectories.

760

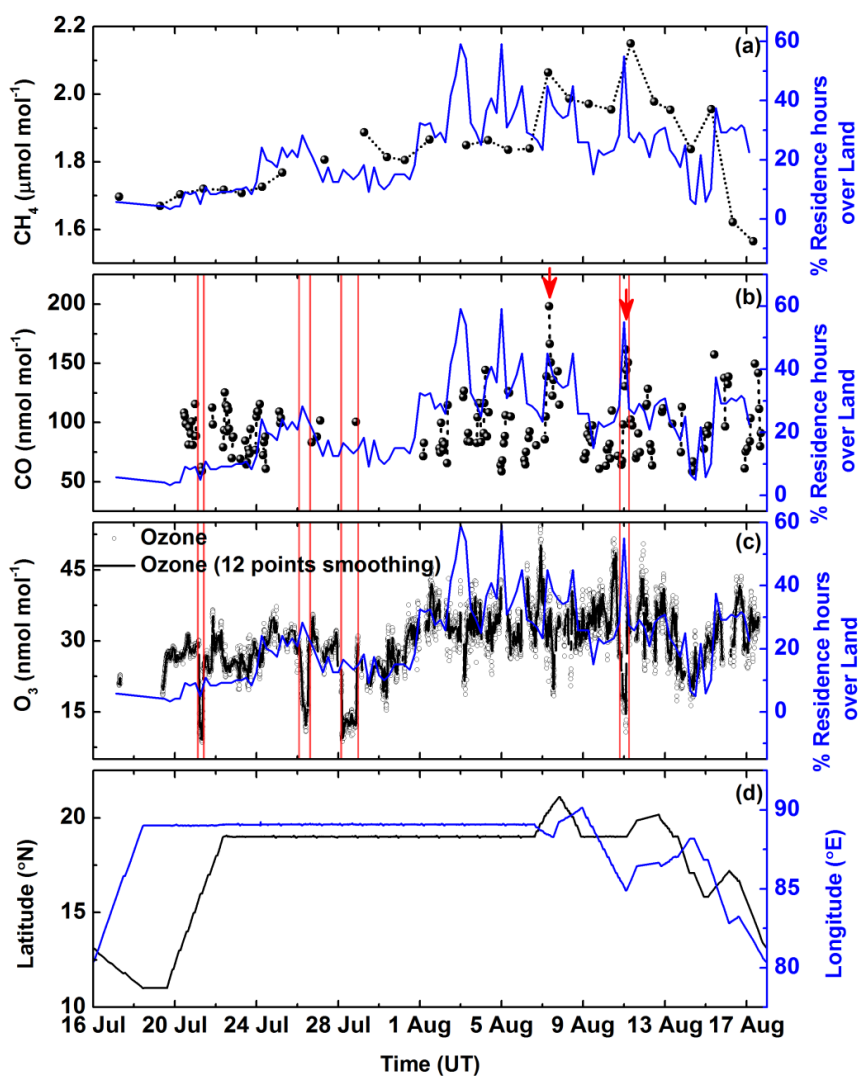
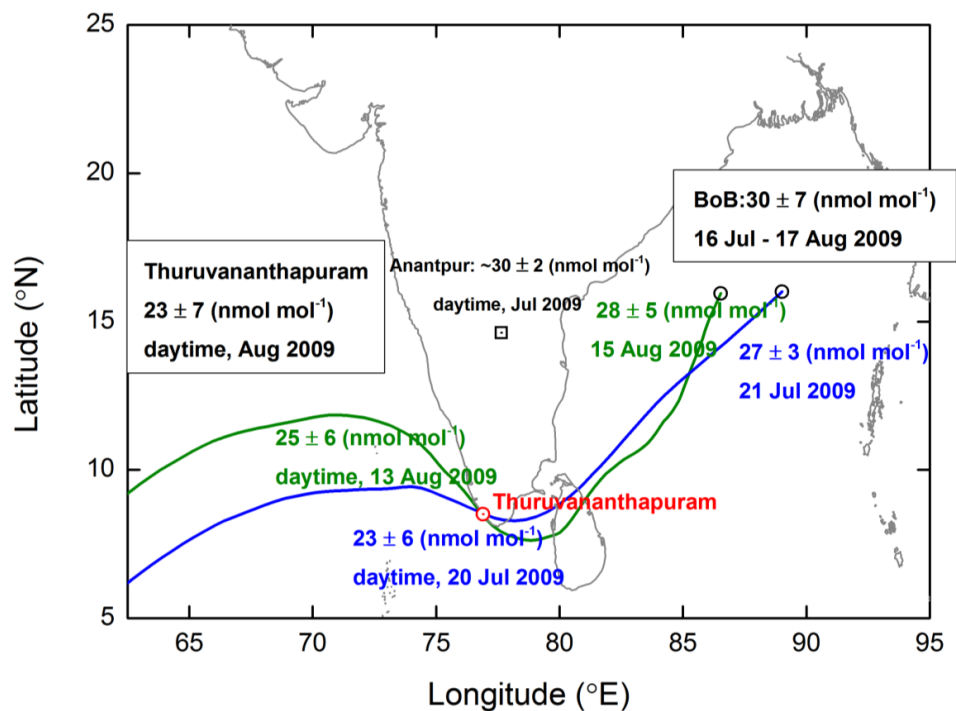
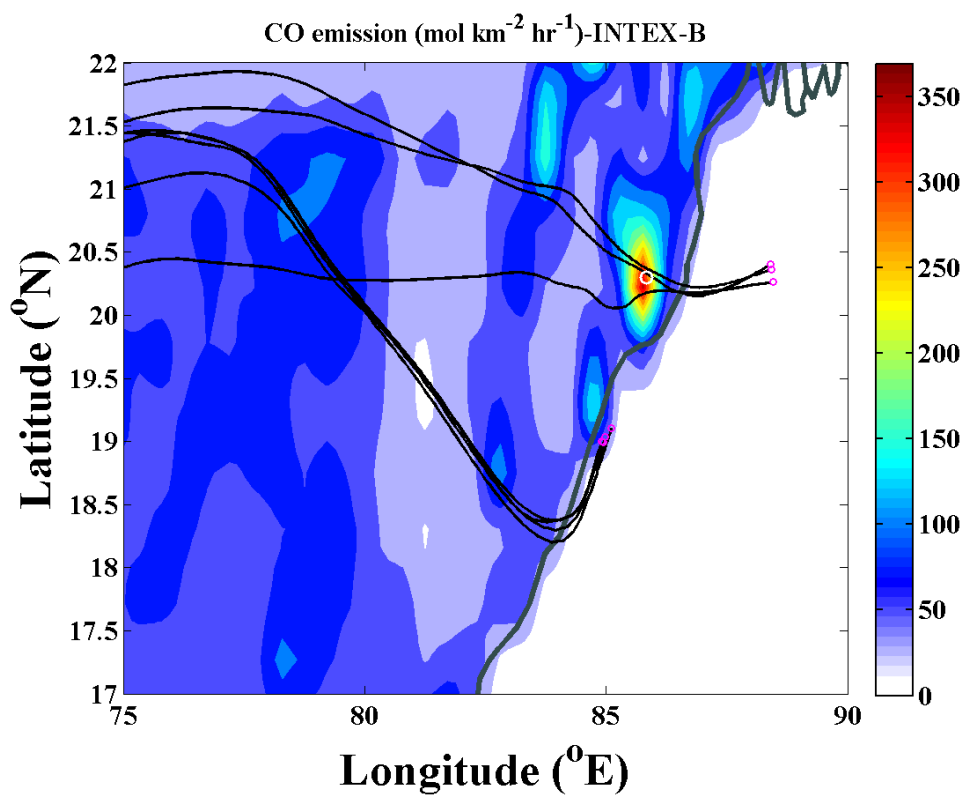


Figure 5. Spatio-temporal variation of surface O_3 (c), CO (b), and CH_4 (a) along with percentage residence time (blue line) over land during the summer monsoon season. The red vertical lines show the four events of sharp decrease in surface O_3 and CO during rainfall (Fig. 11). (d) Variations in measurement locations, latitude (black line), and longitude (blue line) corresponding to trace gas measurements shown in (a–c). Red arrows in 5b highlight elevated CO mixing ratios.



770 **Figure 6.** Airmass back-trajectories (blue and green curves) reaching 500 m altitude over the two locations (black circles) of observations over the BoB for July 21 and August 15, 2009. The trajectories crossed an observational site, Thiruvananthapuram (red circle), on July 20 and August 13, 2009. Monsoon-time average mixing ratios over Thiruvananthapuram (which is representative of the Arabian Sea airmasses), Ananthapur (which is representative of airmasses over the central part of southern India), and the BoB are also shown.



775

Figure 7. Backward Airmass trajectories (black curves) 500 m above the location of higher CO observations as marked by red arrows in Fig. 5b during August 7 and 11, 2009. The background colour map shows the spatial distribution of anthropogenic CO emissions over the Indian region for the year 2006 from INTEX-B inventory. The small circles in magenta represent the points where observations were made, as well as the end-point of trajectories.

780

The white circle over the hot-spot region denotes an observational site, Bhubaneswar.

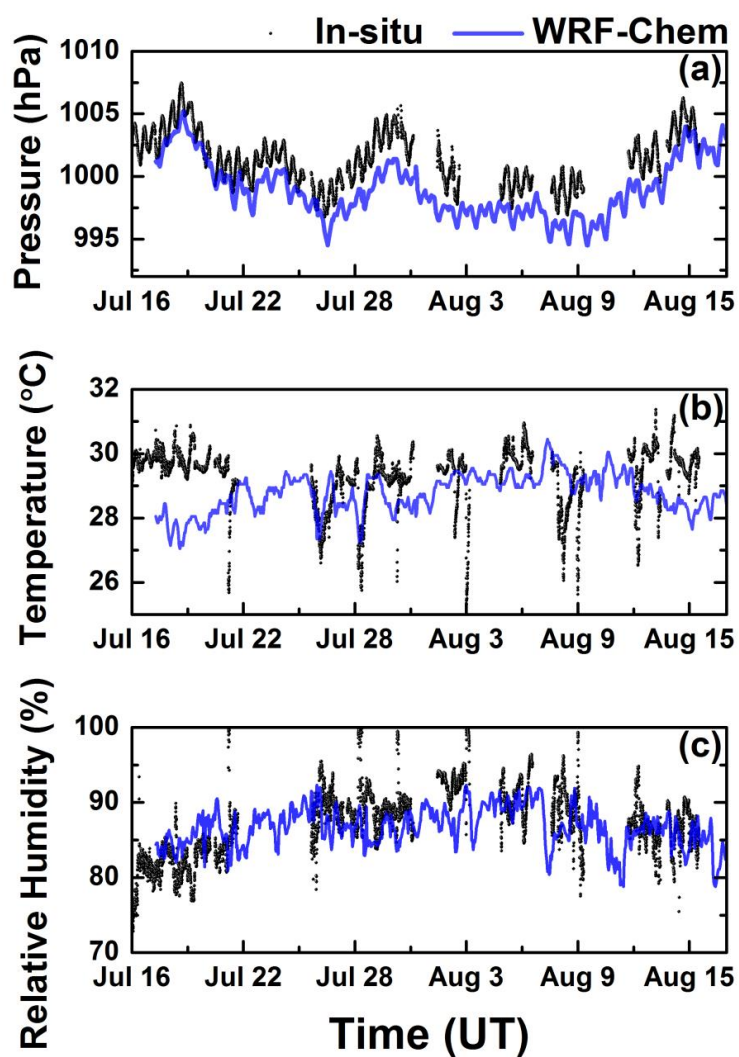


Figure 8. Comparison of the WRF-Chem-simulated meteorological parameters (a) pressure, (b) temperature, and (c) relative humidity with in situ measurements aboard ship during the CTCZ experiment.

785

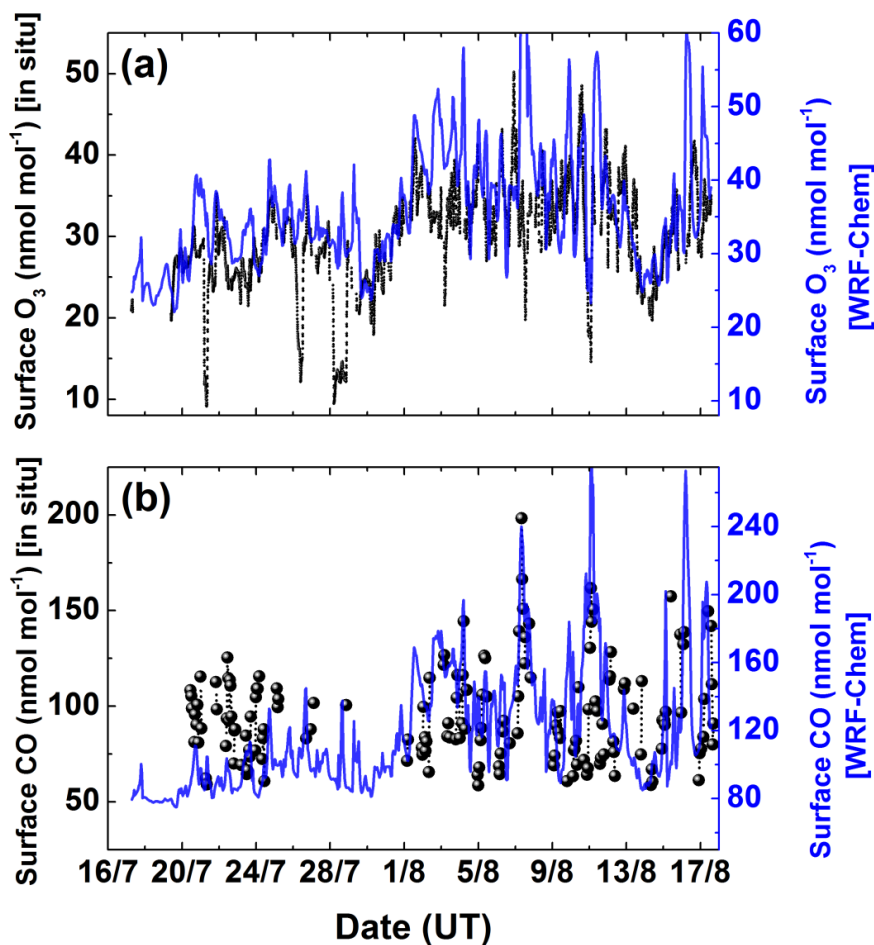


Figure 9. A comparison of surface O_3 and CO from in situ measurements (black dots) with model results from WRF-Chem (blue line) along the cruise track over the BoB during the summer monsoon season. The scale of the right axis is adjusted for WRF-Chem according to the mean biases.

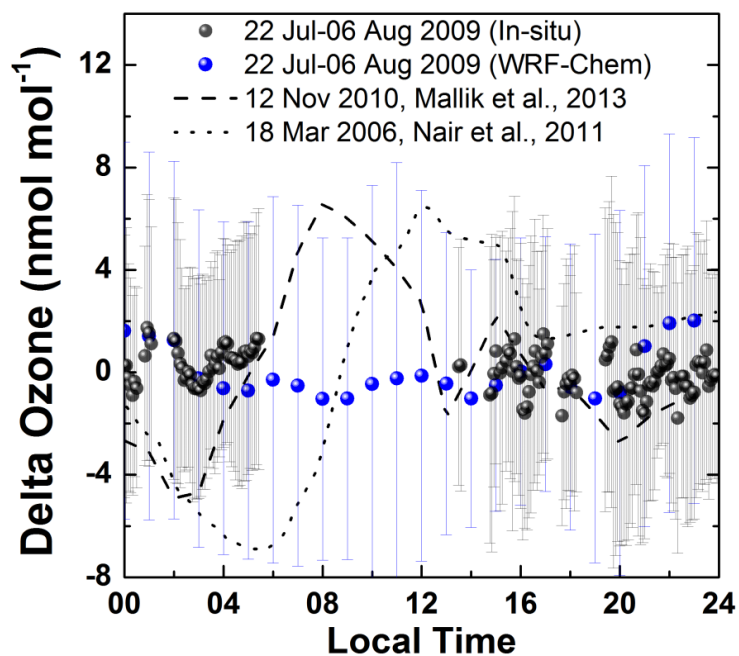


Figure 10. The mean delta-diurnal variation of surface ozone over the BoB at a stationary location (89° E, 19° N) along with that from WRF-Chem simulations during the summer monsoon season. Error bars represent standard deviations. The dotted and dashed curves show diurnal variations in surface O₃ (as adopted from Nair et al., 2011, and Mallik et al., 2013) during the pre-monsoon and post-monsoon seasons, respectively.

795

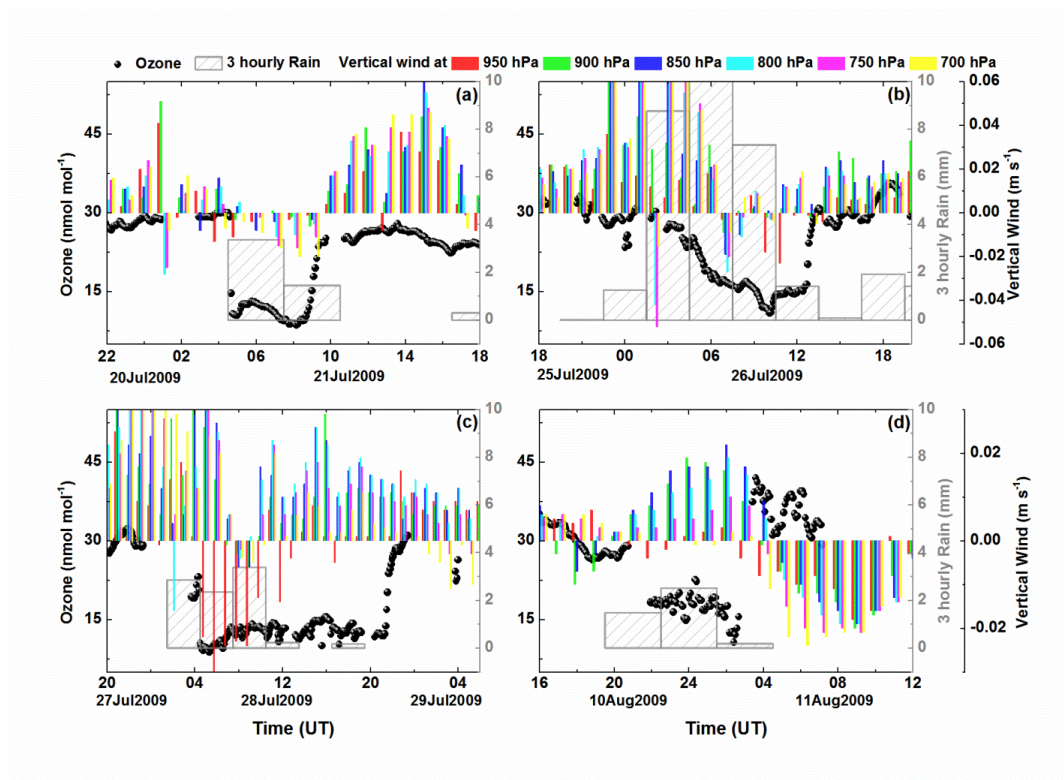


Figure 11. Surface O₃ (black dots) along with 3-hourly rainfall (grey vertical bar) during the four events of sharp decline in ozone (a–d) as marked in Fig. 5c. Colours indicate the vertical wind as simulated by WRF-Chem.

800

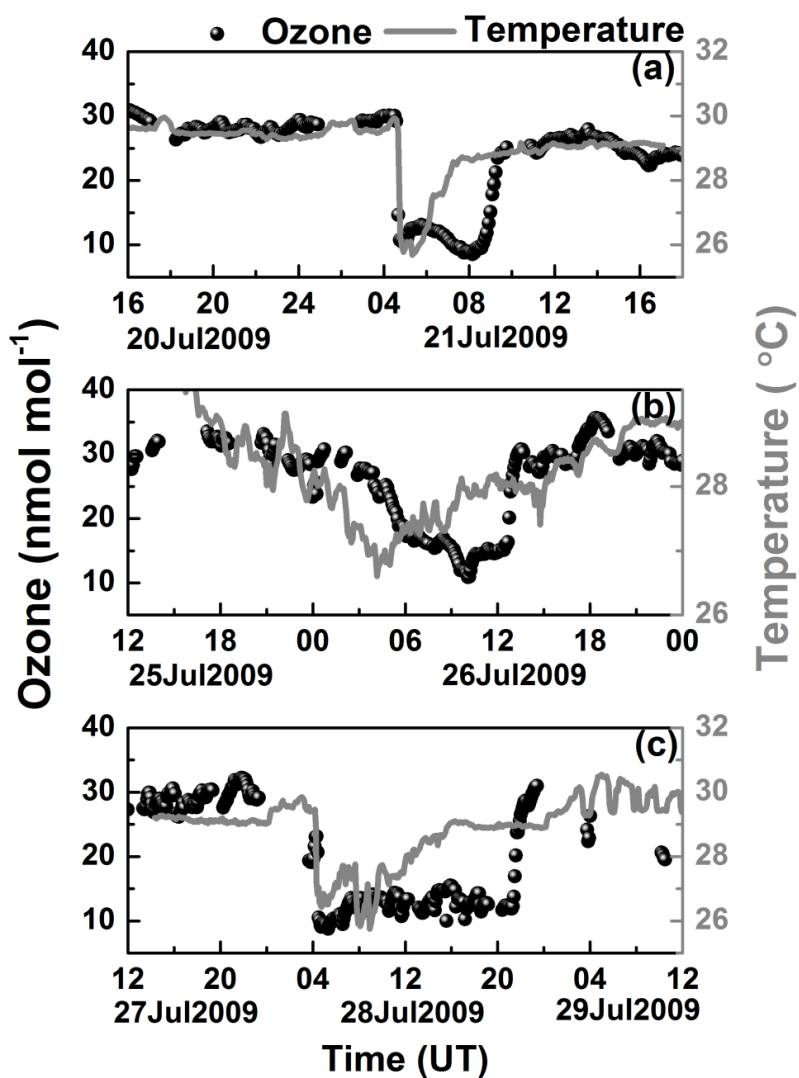
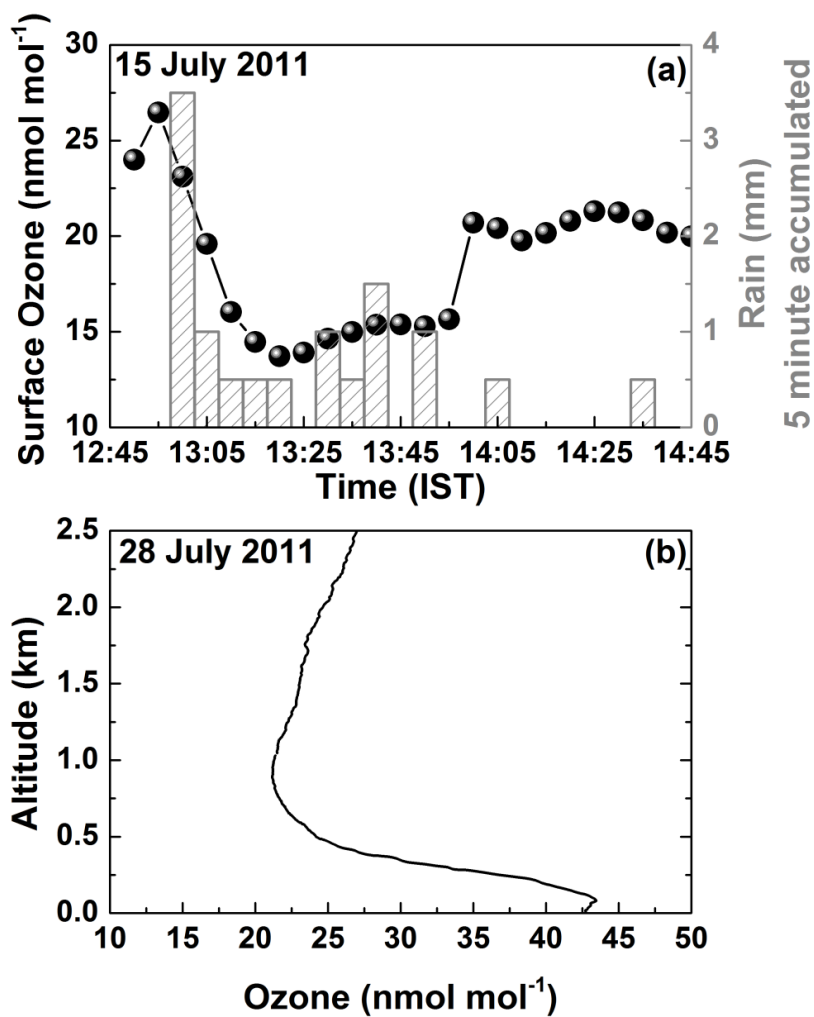
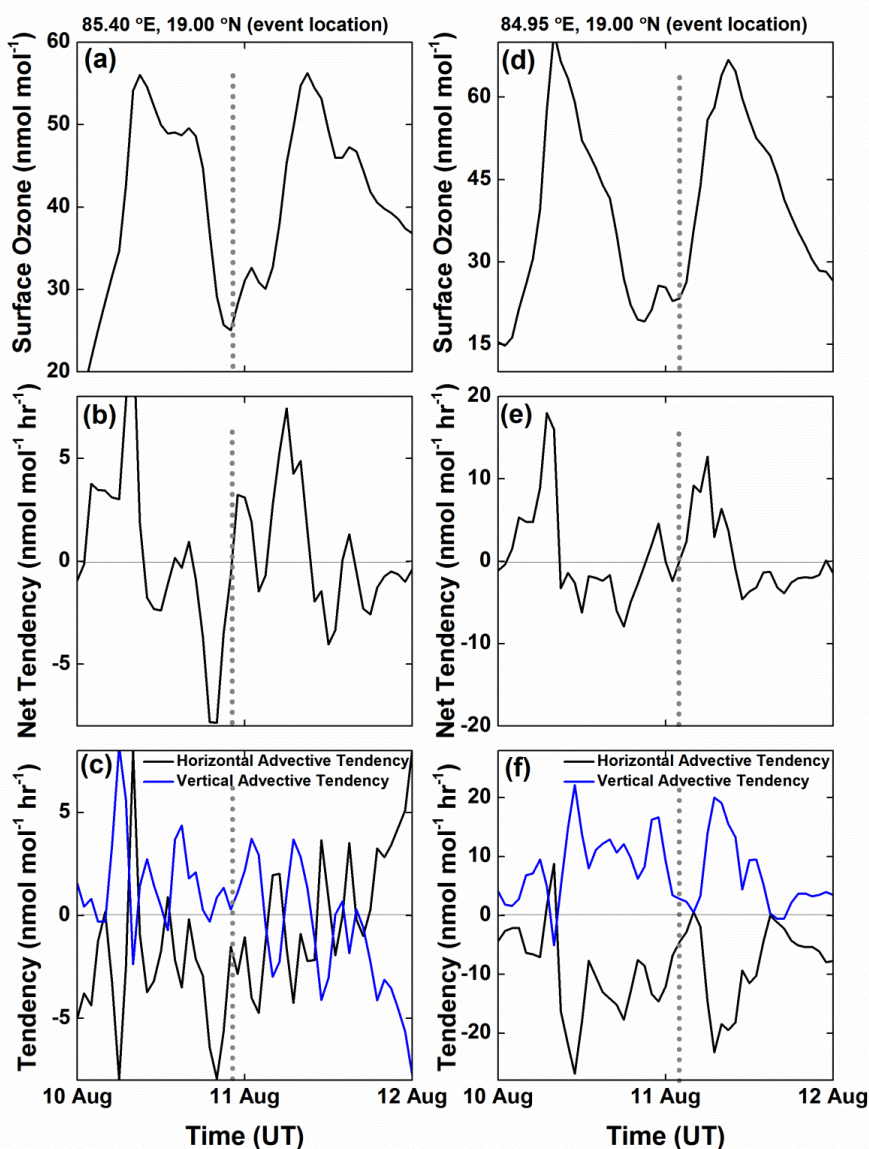


Figure 12. Surface O₃ (black dots) along with surface air temperature (grey line) during the three events of sharp decline in O₃ (a–c) as marked in Fig. 5.



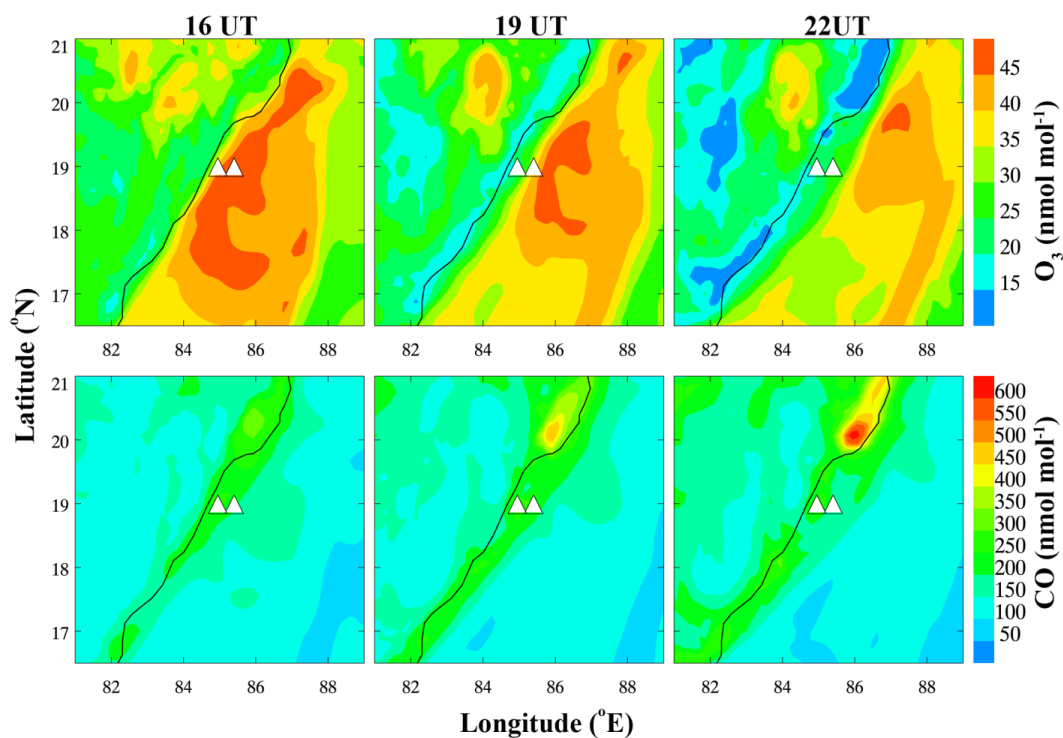
805

Figure 13. (a) Temporal variation in surface O₃ mixing ratio (black dots) along with 5-minute accumulated rainfall (grey vertical bars) over Thumba, Thiruvananthapuram (location of the site shown in Fig. 1 and 2) on 15 July 2011. (b) Vertical profile of O₃ mixing ratio over Thumba, Thiruvananthapuram as measured on 28 July 2011.



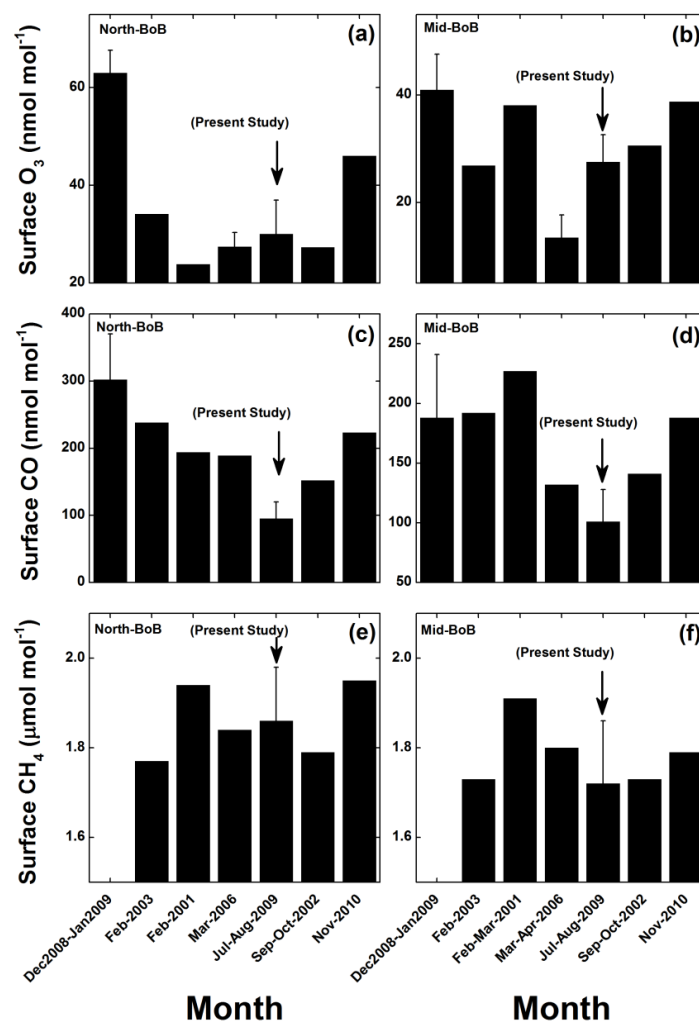
810

Figure 14. Time series of surface O₃ (a) and various tendency terms (b and c) over the event location during the fourth low-ozone event, as obtained from WRF-Chem simulations. 14d–f are the same as 14a–c, but for another location during the same event. These two event locations are also marked by triangles in Figure 15. Vertical dotted line shows the time of the event in the in situ observations of surface O₃ over the indicated locations.



815

Figure 15. Spatial distribution of surface O_3 (top panel) and CO (bottom panel) at 16:00 UT and 19:00 UT on August 10, 2009, both prior to and during the fourth event, which took place 22:00 UT on August 10, 2009. White triangles show two locations ($85.40^\circ E$, $19.00^\circ N$; $84.95^\circ E$, $19.00^\circ N$) corresponding to the event.



820

Figure 16. Seasonal variation in average O₃, CO, and CH₄ mixing ratios over (a, c, e) northern BoB and (b, d, f) central BoB (see Fig. 3 for demarcation of these two regions). Except for July–August 2009 (present study period), all average values are obtained from the literature (David et al., 2011; Lal et al., 2007; Lal et al., 2006; Nair et al., 2011; Srivastava et al., 2012; Sahu et al., 2006; and Mallik et al., 2013). Error bars show standard deviations for respective study periods. For any points for which high resolution measurements are not available, standard deviations are not shown.

825